Table 2. Measurements of 12-Lead ECG of the Patients With Spontaneous Type 1 Brugada ECG

	Diagnosis group	No-diagnosis group	P value
Heart rate (beats/min)	64.4±9.5	68.3±14.7	0.38
PQ interval (ms)	187.4±28.3	161.2±21.5	0.0073
P axis (degrees)	63.9±13.5	58.7±19.5	0.41
QRS axis (degrees)	49.1±44.1	44.9±34.8	0.78
T axis (degrees)	52.8±20.4	59.3±14.0	0.31
QRS-T angle (degrees)	19.8±17.3	27.3±24.0	0.32
QRS-complex duration (ms)	108.4±25.5	103.2±8.6	0.46
QT interval (ms)	398.1±34.9	388.7±33.6	0.45
QTc interval (ms)	409.3±28.2	408.9±17.2	0.96

Table 3. Measurements of Individual Leads of the Patients With Spontaneous Type 1 Brugada ECG

	Diagnosis group	No-diagnosis group	P value
QRS-complex duration in lead V_1 (ms)	101.4±31.6	90.3±19.1	0.25
QRS-complex duration in lead V_2 (ms)	99.0±31.9	88.9±18.1	0.29
QRS-complex duration in lead V_5 (ms)	104.1±27.9	98.3±11.4	0.46
Dispersion of QRS-complex duration (ms)	4.7±14.3	7.9±21.9	0.63
R'-wave amplitude in lead V_1 (μV)	41.3±88.8	94.9±138.4	0.22
R'-wave amplitude in lead V_2 (μV)	90.3±188.5	188.9±248.9	0.23
J-point amplitude in lead V_1 (μV)	183.3±127.9	128.8±78.0	0.17
J-point amplitude in lead V_2 (μV)	311.8±117.6	339.0±135.7	0.55
STM amplitude in lead V_1 (μV)	55.3±66.9	81.7±73.9	0.31
STM amplitude in lead V_2 (μV)	172.1±107.5	192.9±157.8	0.67
Descending amplitude in lead V_1 (μV)	128.0±154.0	47.1±66.6	0.071
T-wave amplitude in lead V_1 (μV)	−170.2±174.6	−43.2±122.3	0.027
T-wave amplitude in lead V_2 (μV)	95.0±363.3	232.1±200.0	0.21
R-wave amplitude in lead aV_R (μV)	104.5±142.8	103.7±101.3	0.99
R/q ratio in lead aV_R	0.35±0.44	0.22±0.20	0.38
R-wave amplitude in lead aV_L (μV)	254.3±281.0	212.7±192.9	0.64
R'-wave amplitude in lead aV_L (μV)	32.2±48.4	49.9±88.4	0.49
R'/q ratio in lead aV_L	0.0±0.0	0.87±1.71	0.20

Dispersion of QRS-complex duration, absolute value of the difference between the QRS-complex duration in leads V_1 and V_5; STM, site at the middle of the ST segment (see Methods); Descending amplitude, difference in the amplitudes at the J-point and STM.

pain, emotional distress, or supine posture, were associated with syncope that was preceded by prodromal symptoms (sweating, nausea, vomiting, yawning). Cardiac transthoracic echocardiography revealed normal left ventricular function without evidence of structural heart disease in all patients of both groups. None of the family members of patients in either group was involved. We performed genetic analysis of 14 of the 16 patients in the diagnosis group, which identified a mutation in *SCN5A* in 1 patient (8.3%) who was a subject of our previous report;[12] no abnormality in *SCN5A* was determined in the remaining 13 patients.

Characteristics of the ECG

Table 2 shows the ECG characteristics. Heart rate did not significantly differ between groups. The PQ interval was significantly longer in the diagnosis group than in the no-diagnosis group; however, there was no significant difference between the 2 groups in the duration of the QRS complex, QT interval, and QTc interval. In addition, the frontal plane axis of the P-, QRS-, and T-wave did not differ between the diagnosis and no-diagnosis group. Table 3 shows the ECG measurements in individual leads. Between the 2 groups,
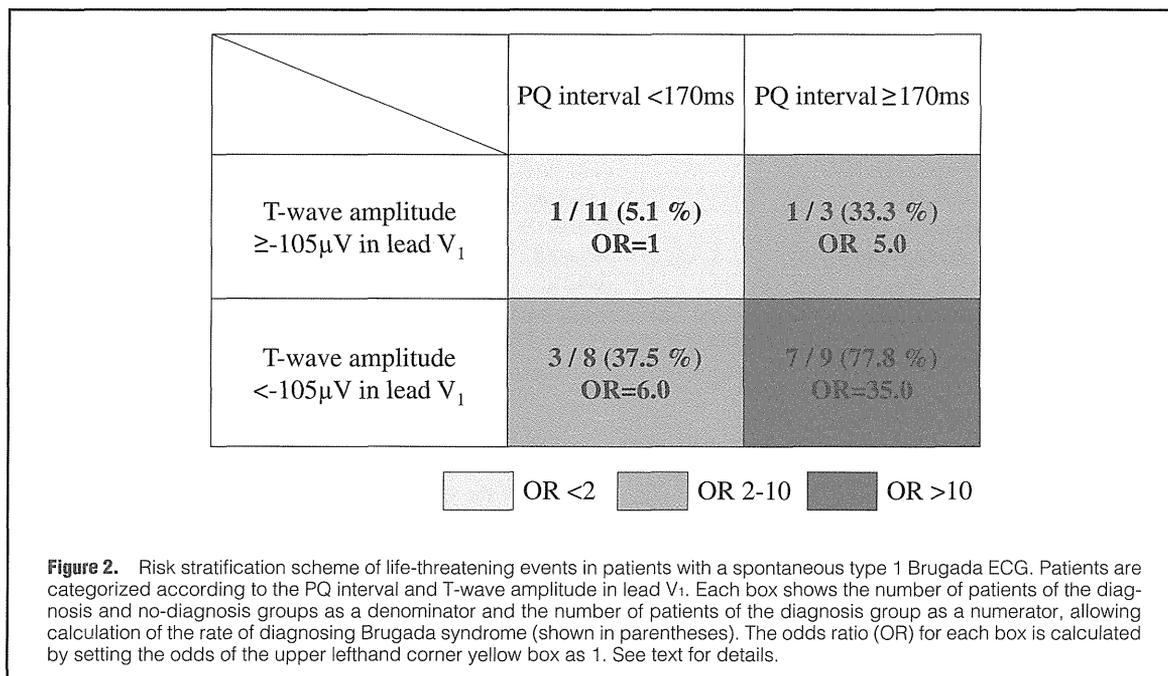
there was no significant difference in the duration of the QRS complex in leads V_1, V_2 and V_5, nor was there in the dispersion of the QRS-complex duration in leads V_1 and V_5, the R'-wave amplitude in leads V_1 and V_2, the J-point amplitude in leads V_1 and V_2, and the STM-amplitude in leads V_1 and V_2. The T-wave in lead V_1 was more negative in the diagnosis group than in the no-diagnosis group, but the T-wave amplitude in lead V_2 was not significantly different between the 2 groups. There was no significant difference between the 2 groups in the other ECG variables, including R-wave amplitude and R/q ratio in lead aV_R, and R-wave amplitude, R'-wave amplitude, and R'/q ratio in lead aV_L.

Risk Stratification

In the patients of the diagnosis and no-diagnosis groups, the factors predictive of life-threatening arrhythmic events were evaluated. Univariate analyses were performed to identify patients at risk of life-threatening events. The presence of a family history, and a PQ interval, and the T-wave amplitude in lead V_1 were significantly associated with BS (Table 4). Multivariate logistic regression analysis revealed that the PQ interval and T-wave amplitude in lead V_1 were indepen-
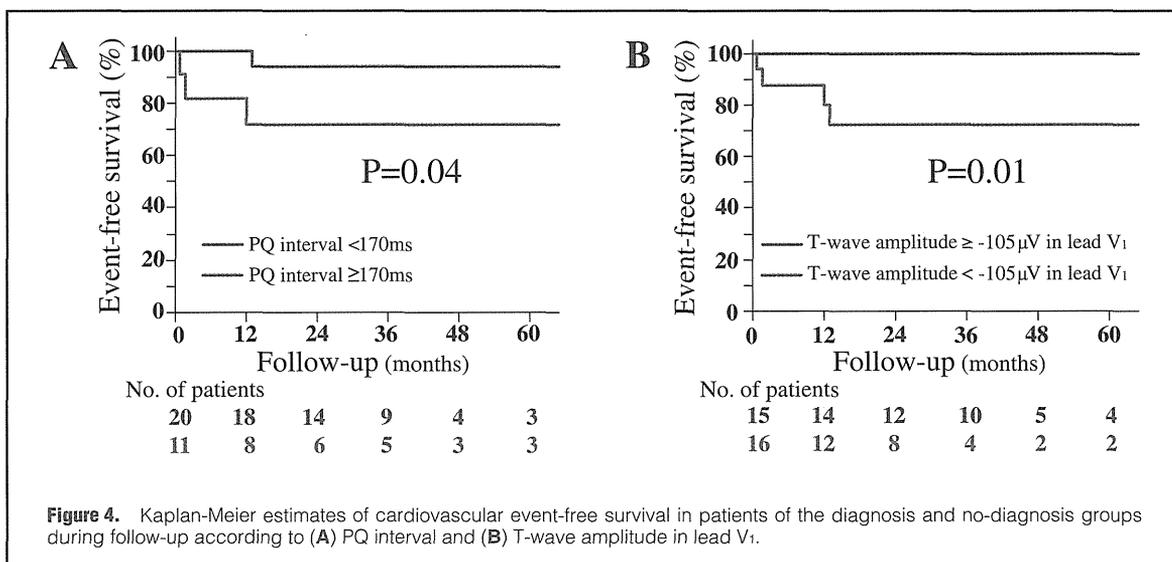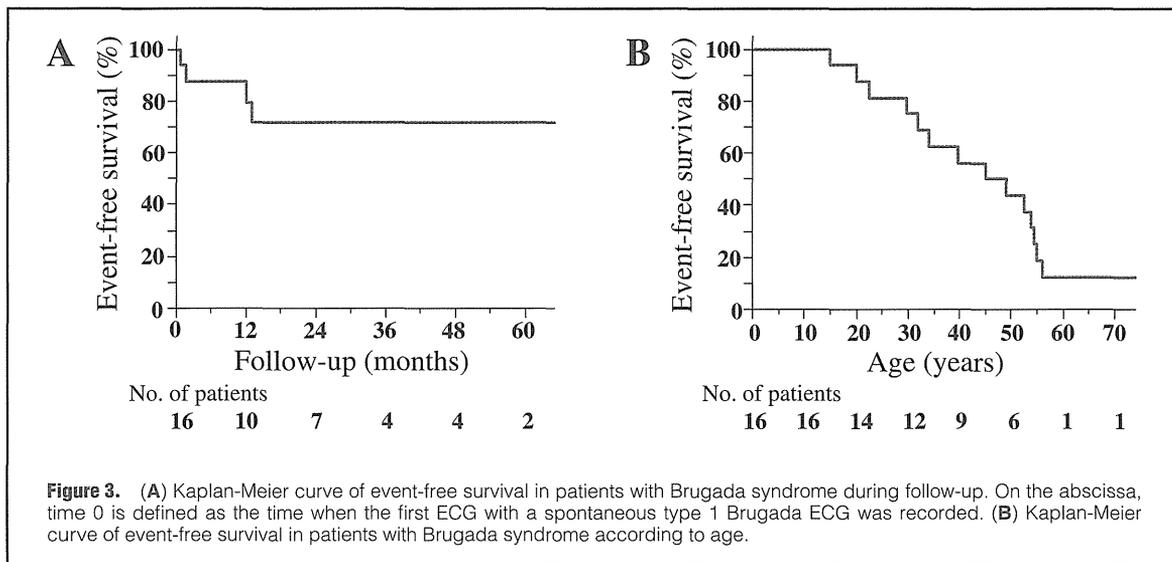
Table 4. Probability of Life-Threatening Arrhythmias According to Clinical and ECG Variables of the Patients With Spontaneous Type 1 Brugada ECG

	P value	Odds ratio	95%CI
Univariate analysis			
Age ≥50 years	0.36	1.93	0.47–8.42
Family history of sudden death	0.043*	10.50	1.47–216.68
Heart rate ≥66 beats/min	0.59	1.47	0.36–6.24
PQ interval ≥170 ms	0.0014*	14.0	2.62–115.18
QTc interval ≥405 ms	0.36	0.52	0.12–2.14
J-point amplitude in V_1 ≥155 μV	0.85	0.86	0.15–3.22
STM amplitude in lead V_1 ≥68 μV	0.58	0.67	0.16–2.76
T-wave amplitude <−105 μV in lead V_1	0.024*	6.05	1.36–32.09
Descending amplitude in lead V_1 ≥49 μV	0.59	1.47	0.36–6.24
Multivariate analysis			
PQ interval ≥170 ms	0.045*	11.50	1.05–268.62
T-wave amplitude <−105 μV in lead V_1	0.037*	8.98	1.14–117.28
Descending amplitude in lead V_1 ≥49 μV	0.19	0.23	0.02–1.94
Family history of sudden death	0.59	2.18	0.12–66.22

Dispersion of QRS-complex duration, absolute value of the difference between the QRS-complex duration in leads V_1 and V_5; STM, site at the middle of the ST segment (see Methods); Descending amplitude, difference in the amplitudes at the J-point and STM.
CI, confidence interval.

Figure 2. Risk stratification scheme of life-threatening events in patients with a spontaneous type 1 Brugada ECG. Patients are categorized according to the PQ interval and T-wave amplitude in lead V_1. Each box shows the number of patients of the diagnosis and no-diagnosis groups as a denominator and the number of patients of the diagnosis group as a numerator, allowing calculation of the rate of diagnosing Brugada syndrome (shown in parentheses). The odds ratio (OR) for each box is calculated by setting the odds of the upper lefthand corner yellow box as 1. See text for details.

dently associated with life-threatening events in patients with a spontaneous type 1 Brugada ECG (Table 4). Figure 2 is a schema for risk stratification constructed according to the values of the PQ interval and T-wave amplitude in lead V_1. Using receiver operating characteristic analysis, the sensitivity and specificity of the PQ interval and T-wave amplitude in lead V_1 in response to life-threatening events were maximized by a PQ interval of 170 ms and a T-wave amplitude of −105 μV in lead V_1. The patients of the diagnosis and no-

diagnosis groups were allocated to 4 categories according to the PQ interval and T-wave amplitude in lead V_1. The rate of diagnosing BS was higher in the category having a PQ interval ≥170 ms than in that of PQ interval <170 ms. The same was true for the categories dichotomized by T-wave amplitude of −105 μV in lead V_1. Furthermore, when present together, the PQ interval and T-wave amplitude in lead V_1 potentiate each other, leading to a diagnosis of BS that is substantially greater than that of its individual components.

Figure 3. (A) Kaplan-Meier curve of event-free survival in patients with Brugada syndrome during follow-up. On the abscissa, time 0 is defined as the time when the first ECG with a spontaneous type 1 Brugada ECG was recorded. (B) Kaplan-Meier curve of event-free survival in patients with Brugada syndrome according to age.

Figure 4. Kaplan-Meier estimates of cardiovascular event-free survival in patients of the diagnosis and no-diagnosis groups during follow-up according to (A) PQ interval and (B) T-wave amplitude in lead V₁.

Long-Term Outcome

Figure 3A shows the Kaplan-Meier survival curve of life-threatening events in the diagnosis group after a type 1 Brugada ECG was recorded. During the follow-up, 6 of the 15 patients (40%) who received an ICD experienced recurrence of life-threatening arrhythmic events. No patient died in the diagnosis group during follow-up. The duration from the diagnosis of BS to recurrence of life-threatening events ranged from 0.7 to 74 months (mean, 28.9±34.6 months). Approximately 30% of patients had recurrence within 1 year (**Figure 3A**). **Figure 3B** shows the age-dependent event-free survival curve of life-threatening events in the diagnosis group. Life-threatening events occurred between 15 and 60 years of age. A comparison of the ECG variables of patients with ICD intervention with those of patients without an ICD

in the diagnosis group was made (**Table S1**). Heart rate was significantly faster in patients with an ICD than in those without, and the PQ interval was significantly longer in patients with an ICD than in those without. However, other ECG variables did not differ between patients with and without an ICD.

On the basis of the significant association of PQ interval and negative T wave in lead V₁ with BS, as shown in **Table 4**, the life-threatening event-free rate was estimated for the patients in both groups according to PQ interval and T-wave amplitude in lead V₁. **Figure 4** shows the Kaplan-Meier life-table analysis. The PQ interval was associated with a significant (P=0.04) difference in the life-threatening event-free rate between patients (n=11) with a PQ interval ≥170 ms and those (n=20) with a PQ interval <170 ms (haz-

ard ratio, 6.9; 95%CI, 1.1–133.5) (Figure 4A). In addition, the T-wave amplitude in lead V_1 was associated with a significant (P=0.013) difference in the life-threatening event-free rate between patients (n=16) with an amplitude $<-105\mu V$ and those (n=15) with an amplitude $\geq-105\mu V$ (hazard ratio, not available [because of the lack of events in patients with a T-wave amplitude in lead $V_1 \geq-105\mu V$]) (Figure 3B). Because none of the patients in the no-diagnosis group had a life-threatening event, multivariate survival analysis could not be performed.

Discussion

To utilize the convenience of the 12-lead ECG, a spontaneous type 1 Brugada ECG was used to enroll patients in this study. By conducting a computer-processed analysis, the discriminative ECG features of patients diagnosed with BS (diagnosis group), compared with patients not diagnosed with BS (no-diagnosis group), were found. First, atrial conduction was delayed in patients diagnosed with BS as compared with the no-diagnosis group. Second, the T-wave in lead V_1 was more negative in patients diagnosed with BS. Third, the duration of the QRS-complex in the right precordial leads did not show a significant difference between the diagnosed and undiagnosed patients. In addition, the amplitude of the R'-wave, J-point, and STM in the right precordial leads did not show a significant difference between the diagnosed and undiagnosed patients. These ECG findings are novel for differentiating patients at risk of developing life-threatening arrhythmia among patients who show a spontaneous type 1 Brugada ECG. Moreover, the risk-stratification schemes elaborated in this study revealed the patients who needed an ICD.

Risk Determinants

In BS, the transient outward current (I_{to})-mediated phase 1 is much more prominent in the epicardium than in the endocardium, leading to ST-segment elevation in the right precordial leads.[11] However, our data from the present study showed there was no significant difference in either the J-point amplitude or the ST-segment amplitude in the right precordial leads between patients diagnosed or not diagnosed with BS. There are several reasons for this: (1) we enrolled patients with a J-point amplitude ≥2 mm and coved-type ST-segment elevation, (2) the ST-segment elevation could be due to ion channel abnormalities such as a reduction of sodium and calcium currents, and (3) a clinically veiled histological abnormality may affect ventricular repolarization. In contrast to the amplitude of the J-point and the ST segment, the T-wave in lead V_1 was more negative in patients diagnosed with BS than in the undiagnosed patients. This finding is compatible with the inward calcium current overcoming the outward I_{to} during phases 1 and 2, causing a secondary depolarization in the epicardial action potential. Besides, the balance of the 2 ionic currents reverses as the I_{to} current overwhelms the calcium current, resulting in a loss of the action potential dome and an abbreviation of the action potential duration that lead to phase 2 reentry.[13] Consistent with these fundamental mechanisms, Nagase et al[14] demonstrated that prolongation of the epicardial action potential following I_{to}-mediated accentuation of the action potential in the right ventricular outflow tract caused the T-wave in the right precordial leads to become negative, coinciding with a type 1 Brugada ECG. In addition, dynamic instability depicted by the restitution property of the action potential

duration in the right ventricular outflow tract may contribute to the occurrence of reentry.[15]

Though the patients diagnosed with BS did not show significant intraventricular conduction delay in the right ventricle, which was different from a previous report,[16] the atrial conduction delay was more pronounced in the diagnosed patients than in the undiagnosed patients. It has been reported that there is an increased atrial vulnerability to fibrillation in BS.[17,18] In those reports, the inter- and intra-atrial conduction delays were associated with atrial fibrillation. In the present study, the PQ interval was longer in the diagnosis group than in the no-diagnosis group, but the QRS-complex duration did not differ between the 2 groups. These findings suggest that a conduction disturbance occurred in the atrium and/or the atrioventricular node rather than in the ventricle. In fact, atrial fibrillation occurred only in 1 patient of each group during the follow-up. We should therefore pay close attention to examining whether atrial fibrillation develops. Furthermore, a P-wave abnormality[19] and a high prevalence of sick sinus syndrome[20] complicated by BS indicate atrial involvement.

Long-Term Prognosis

Brugada et al showed that symptomatic and asymptomatic patients with ST-segment elevation in the right precordial leads shared a similar incidence of cardiac arrest.[21] Other investigators[6,7] also reported that asymptomatic patients with such an ECG characteristic were at risk for sudden death, although the event-free survival rate in those studies was much lower than that of patients in the "Brugada" registry.[13] In contrast, sudden death did not occur in any of patients of the no-diagnosis group and asymptomatic group in our study. This result may be related to not involving family members of proband in the study.

Similar to previous reports,[6,7] we found that most patients of the diagnosis group suffered from ventricular tachyarrhythmia or syncope of unknown origin and approximately one-third patients of the diagnosis group had a recurrence of ventricular tachyarrhythmia. In contrast, none of patients not diagnosed with BS (no-diagnosis group) had sudden death or ventricular tachyarrhythmia. Thus, we emphasize again the importance of medical history-taking: syncope and family history of sudden death.

Study Limitations

First, the ST-segment elevation is not constantly observed in BS patients, because of the so-called "wax and wane" phenomenon, therefore patients with an ST-segment elevation $<0.2\,mV$ at the J-point were missed even if they had BS. Second, because of the limited follow-up, it cannot be assumed that asymptomatic patients did not develop SCD. Third, the response bias of the questionnaire should be considered. We must pay further attention to assessing the long-term prognosis in asymptomatic patients with a spontaneous type 1 Brugada ECG.

Study Implications

Despite the fact that a spontaneous type 1 Brugada ECG is diagnostic, the discriminative ECG features associated with a risk for SCD remain undetermined. From the results of the present study, we propose the PQ interval and negative T wave in lead V_1 as valuable ECG markers of BS. In addition, we underscore that medical information, including the family history, is helpful in the management of patients with a spontaneous type 1 Brugada ECG. It may be possible to deduce

the ECG features presented here to locate subjects in wide populations, such as health examinations, who are at risk.

Disclosures

No conflicts to disclose.

References

1. Brugada P, Brugada J. Right bundle branch block, persistent ST segment elevation and sudden cardiac death: A distinct clinical and electrocardiographic syndrome: A multicenter report. *J Am Coll Cardiol* 1992; **20:** 1391–1396.
2. Antzelevitch C, Brugada P, Borggrefe M, Brugada J, Brugada R, Corrado D, et al. Brugada syndrome: Report of the second consensus conference: Endorsed by the heart rhythm society and the european heart rhythm association. *Circulation* 2005; **111:** 659–670.
3. Miyasaka Y, Tsuji H, Yamada K, Tokunaga S, Saito D, Imuro Y, et al. Prevalence and mortality of the Brugada-type electrocardiogram in one city in japan. *J Am Coll Cardiol* 2001; **38:** 771–774.
4. Matsuo K, Akahoshi M, Nakashima E, Suyama A, Seto S, Hayano M, et al. The prevalence, incidence and prognostic value of the Brugada-type electrocardiogram: A population-based study of four decades. *J Am Coll Cardiol* 2001; **38:** 765–770.
5. Brugada J, Brugada R, Antzelevitch C, Towbin J, Nademanee K, Brugada P. Long-term follow-up of individuals with the electrocardiographic pattern of right bundle-branch block and ST-segment elevation in precordial leads V1 to V3. *Circulation* 2002; **105:** 73–78.
6. Priori SG, Napolitano C, Gasparini M, Pappone C, Della Bella P, Giordano U, et al. Natural history of Brugada syndrome: Insights for risk stratification and management. *Circulation* 2002; **105:** 1342–1347.
7. Eckardt L, Probst V, Smits JP, Bahr ES, Wolpert C, Schimpf R, et al. Long-term prognosis of individuals with right precordial ST-segment-elevation brugada syndrome. *Circulation* 2005; **111:** 257–263.
8. Brugada P, Brugada R, Brugada J. Should patients with an asymptomatic Brugada electrocardiogram undergo pharmacological and electrophysiological testing? *Circulation* 2005; **112:** 279–292; discussion 279–292.
9. Priori SG, Napolitano C. Should patients with an asymptomatic Brugada electrocardiogram undergo pharmacological and electrophysiological testing? *Circulation* 2005; **112:** 279–292; discussion 279–292.
10. Chen Q, Kirsch GE, Zhang D, Brugada R, Brugada J, Brugada P, et al. Genetic basis and molecular mechanism for idiopathic ventricular fibrillation. *Nature* 1998; **392:** 293–296.
11. Makiyama T, Akao M, Shizuta S, Doi T, Nishiyama K, Oka Y, et al. A novel scn5a gain-of-function mutation M1875T associated with familial atrial fibrillation. *J Am Coll Cardiol* 2008; **52:** 1326–1334.
12. Kawamura M, Ozawa T, Yao T, Ashihara T, Sugimoto Y, Yagi T, et al. Dynamic change in ST-segment and spontaneous occurrence of ventricular fibrillation in Brugada syndrome with a novel nonsense mutation in the SCN5A gene during long-term follow-up. *Circ J* 2009; **73:** 584–588.
13. Yan GX, Antzelevitch C. Cellular basis for the Brugada syndrome and other mechanisms of arrhythmogenesis associated with ST-segment elevation. *Circulation* 1999; **100:** 1660–1666.
14. Nagase S, Kusano KF, Morita H, Nishii N, Banba K, Watanabe A, et al. Longer repolarization in the epicardium at the right ventricular outflow tract causes type 1 electrocardiogram in patients with Brugada syndrome. *J Am Coll Cardiol* 2008; **51:** 1154–1161.
15. Ashino S, Watanabe I, Kofune M, Nagashima K, Ohkubo K, Okumura Y, et al. Abnormal action potential duration restitution property in the right ventricular outflow tract in Brugada syndrome. *Circ J* 2010; **74:** 664–670.
16. Kanda M, Shimizu W, Matsuo K, Nagaya N, Taguchi A, Suyama K, et al. Electrophysiologic characteristics and implications of induced ventricular fibrillation in symptomatic patients with Brugada syndrome. *J Am Coll Cardiol* 2002; **39:** 1799–1805.
17. Morita H, Kusano-Fukushima K, Nagase S, Fujimoto Y, Hisamatsu K, Fujio H, et al. Atrial fibrillation and atrial vulnerability in patients with Brugada syndrome. *J Am Coll Cardiol* 2002; **40:** 1437–1444.
18. Kusano KF, Taniyama M, Nakamura K, Miura D, Banba K, Nagase S, et al. Atrial fibrillation in patients with Brugada syndrome relationships of gene mutation, electrophysiology, and clinical backgrounds. *J Am Coll Cardiol* 2008; **51:** 1169–1175.
19. Yamada T, Watanabe I, Okumura Y, Takagi Y, Okubo K, Hashimoto K, et al. Atrial electrophysiological abnormality in patients with Brugada syndrome assessed by P-wave signal-averaged ECG and programmed atrial stimulation. *Circ J* 2006; **70:** 1574–1579.
20. Hayashi H, Sumiyoshi M, Yasuda M, Komatsu K, Sekita G, Kawano Y, et al. Prevalence of the Brugada-type electrocardiogram and incidence of Brugada syndrome in patients with sick sinus syndrome. *Circ J* 2010; **74:** 271–277.
21. Brugada J, Brugada R, Brugada P. Right bundle-branch block and ST-segment elevation in leads V1 through V3: A marker for sudden death in patients without demonstrable structural heart disease. *Circulation* 1998; **97:** 457–460.

Supplemental Files

Supplemental File 1

Figure S1. 12-lead ECG of a 49-year-old man who was diagnosed with Brugada syndrome.

Figure S2. 12-lead ECG of a 55-year-old man who was undiagnosed with Brugada syndrome.

Table S1. Comparison of ECG Variables Between Patients With and Without ICD Intervention in the BS Diagnosis Group

Please find supplemental file(s);
http://dx.doi.org/10.1253/circj.CJ-10-0903

KCNE5 (KCNE1L) Variants Are Novel Modulators of Brugada Syndrome and Idiopathic Ventricular Fibrillation

Seiko Ohno, MD, PhD*; Dimitar P. Zankov, MD, PhD*; Wei-Guang Ding, MD, PhD; Hideki Itoh, MD, PhD; Takeru Makiyama, MD, PhD; Takahiro Doi, MD; Satoshi Shizuta, MD; Tetsuhisa Hattori, MD; Akashi Miyamoto, MD; Nobu Naiki, MD; Jules C. Hancox, PhD; Hiroshi Matsuura, MD, PhD; Minoru Horie, MD, PhD

Background—Brugada syndrome (BrS) has a significantly higher incidence among the male sex. Among genes coding ion channels and their modulatory proteins, *KCNE5* (*KCNE1L*) is located in the X chromosome and encodes an auxiliary β-subunit for K channels. KCNE5 has been shown to modify the transient outward current (I_{to}), which plays a key role in determining the repolarization process in the myocardium. This study investigated whether *KCNE5* mutations could be responsible for BrS and other idiopathic ventricular fibrillation (IVF).

Methods and Results—In 205 Japanese patients with BrS or IVF who tested negative for *SCN5A* mutation, we conducted a genetic screen for *KCNE5* variants. We identified 2 novel *KCNE5* variants: p.Y81H in 3 probands and p.[D92E;E93X] in 1 proband from 4 unrelated families. Y81H was identified in 1 man and 2 women; D92E;E93X was found in a 59-year-old man. All probands received implantable cardioverter-defibrillators. Functional consequences of the *KCNE5* variants were determined through biophysical assay using cotransfection with *KCND3* or *KCNQ1*. In the experiments with *KCND3*, which encodes Kv4.3, I_{to} was significantly increased for both *KCNE5* variants compared to wild type. In contrast, there were no significant changes in current properties reconstructed by *KCNQ1*+wild type *KCNE5* and the 2 variants. With the simulation model, both variants demonstrated notch-and-dome or loss-of-dome patterns.

Conclusions—KCNE5 modulates I_{to}, and its novel variants appeared to cause IVF, especially BrS, in male patients through gain-of-function effects on I_{to}. Screening for *KCNE5* variants is relevant for BrS or IVF. (***Circ Arrhythm Electrophysiol. 2011;4:352-361.***)

Key Words: KCNE5 protein human ■ KCNE1L protein human ■ Brugada syndrome ■ idiopathic ventricular fibrillation

B rugada syndrome (BrS) is a clinical entity presenting ST-segment elevation in the right precordial ECG leads and a high incidence of sudden death due to idiopathic ventricular fibrillation (IVF).[1] Its incidence rate is 8- to 10-fold higher in the male sex.[2] However, the mechanism underlying this sex difference remains unknown. In 1998, *SCN5A*, a gene encoding the α-subunit of cardiac Na channels, was reported as the causative gene for BrS.[3] *SCN5A* mutations cause a reduction of cardiac Na current, which increases transmural dispersion of action potential (AP) duration in the right ventricle, thereby inducing the characteristic ST elevation seen on ECG and arrhythmogenicity. However, *SCN5A* mutations were identified in only 20% to 30% of patients.[4] Additional candidates *GPD1L*,[5] *CACNA1C*, *CACNB2*,[6] *SCN1B*,[7] *KCNE3*,[8] and *KCNQ1*[9] have been reported, but supposedly, they are not major causative genes in BrS. We identified *SCN5A* mutations in only 4 (10.5%) of 38 patients with BrS,[10] and none in *GPD1L*,[11] *KCNQ1*, or *KCNE3* in the same patient group. Therefore, some genes responsible for BrS may remain unidentified.

Clinical Perspective on p 361

According to previous studies, the characteristic ST elevation in right precordial leads could be induced either by reduction in Na current or L-type calcium channel current or increased in transient outward currents (I_{to}). Blockade of I_{to} by 4-aminopyridine causes a loss of AP dome in the epicardium of canine wedge preparation,[12] and activation of I_{to} by NS5806 has been shown to recapitulate the electrographic and arrhythmic manifestation of BrS.[13] In humans, I_{to} supposedly comprises Kv4.3 and Kv channel-interacting protein (KChIP2),[14] and β-subunits encoded by the *KCNE* family

affect I_{to}.[15] Among *KCNE* family members, *KCNE5* (*KCNE1L*) is located on the X chromosome[16] and, therefore, may be involved in sex differences. Indeed, a polymorphism, 97T, in *KCNE5* may afford protection against atrial fibrillation (AF) and contribute to sex differences in AF.[17] Therefore, we screened extensively for *KCNE5* variants in 205 consecutive probands with BrS, IVF, or both and identified 2 novel *KCNE5* variants in 4 unrelated families. Both variants were studied using heterologous coexpression with Kv4.3/KChIP2 in Chinese hamster ovary (CHO) cells.

Methods

Patients
Study patients comprised 205 probands with BrS or IVF from unrelated families. They were referred consecutively to either of our laboratories for genetic evaluation. All subjects submitted written informed consent in accordance with the guidelines approved by each institutional review board. Each underwent detailed clinical and cardiovascular examinations.

Genotyping
Genomic DNA was isolated from venous blood lymphocytes as previously described.[18] Through polymerase chain reaction, denaturing high-performance liquid chromatography (DHPLC), and direct DNA sequencing, we performed a comprehensive open reading frame and splice-site mutational analysis of known BrS-related genes (*KCNQ1*, *SCN5A*, *KCNE2*, *KCNE3*, *GPD1L*, and *SCN1B*) and *KCNE5* using previously described primers.[5,7,10,18–20] Although we did not examine *CACNA1C* and *CACNB2* because the patients had no QT shortening in their ECGs, we checked known mutations in the Ca channels once a change in *KCNE5* was identified in a proband. DHPLC analysis for *KCNE5* was performed by mixing 2 samples to detect hemizygous or homozygous mutations. Denaturing temperatures of DHPLC were 65°C and 67°C. The cDNA sequence was based on GenBank reference sequence NM_012282, and the numbering reflects cDNA numbering, with +1 corresponding to the A of the ATG translation initiation codon in the reference sequence. The initiation codon is codon 1.

Plasmid Construction
The complete coding region of *KCNE5* was amplified using polymerase chain reaction from human genomic DNA of patients and controls and cloned into a pIRES-CD8 vector that we previously constructed.[21] Nucleotide sequence analysis of the *KCNE5* coding region was performed on each variant construct before the expression study. Full-length cDNA encoding the short isoform of human *KCND3* subcloned into the pIRES-GFP (Clontech; Palo Alto, CA) expression vector was provided by Dr G. F. Tomaselli (The Johns Hopkins University; Baltimore, MD). Full-length cDNA encoding KChIP2 subcloned into the PCMV-IRS expression vector was a gift from Dr G.-N. Tseng (Virginia Commonwealth University; Richmond, VA). Full-length cDNAs for human *KCNQ1* and *KCNE1* were provided by Dr. J. Barhanin (Institut de Pharmacologie Moléculaire et Cellulaire, CNRS, Valbonne, France) and subcloned into pIRES2-EGFP and pIRES-CD8 vectors, respectively, as previously reported.[18]

Mammalian Cell Line and cDNA Transfection
CHO cells were transiently cotransfected with cDNA of *KCND3*, *KChIP2*, and wild type (WT) or variants (Y81H or D92E;E93X) of *KCNE5* at equimolar concentrations (1.5 μg *KCND3*, 1 μg *KChIP2*, and 1.5 μg *KCNE5*) using Lipofectamine (Invitrogen Life Technologies; Carlsbad, CA). In a subset of experiments, WT or *KCNE5* variants also were cotransfected into cells with 0.5 μg *KCNQ1* and 0.5 μg *KCNE1* (subcloned to pCI vector).

Patch-Clamp Recordings and Data Analysis
Whole-cell membrane currents were recorded with an EPC-8 patch-clamp amplifier (HEKA Elektronik; Lambrecht, Germany). Data were low-pass filtered at 1 kHz, acquired at 5 kHz through an LIH-1600 analog-to-digital converter (HEKA Elektronik), and stored on a computer hard drive using Patchmaster software (HEKA Elektronik). The extracellular solution contained 140 mmol/L NaCl, 5.4 mmol/L KCl, 1.8 mmol/L $CaCl_2$, 0.5 mmol/L $MgCl_2$, 0.33 mmol/L NaH_2PO_4, 5.5 mmol/L glucose, and 5.0 mmol/L Hepes (pH 7.4 with NaOH). Patch pipettes were fabricated from borosilicate glass capillaries (Narishige; Tokyo, Japan) on a horizontal microelectrode puller (P-97; Sutter Instrument Co; Novato, CA), and the tips were fire-polished using microforge. Patch pipettes had a resistance of 3.0 to 4.0 MΩ when filled with the pipette solution containing 70 mmol/L potassium aspartate, 50 mmol/L KCl, 10 mmol/L KH_2PO_4, 1 mmol/L $MgSO_4$, 3 mmol/L Na_2-ATP (Sigma), 0.1 mmol/L Li_2-GTP (Roche Diagnostics GmbH; Mannheim, Germany), 5 mmol/L EGTA, and 5 mmol/L Hepes (pH 7.2).

Forty-eight hours after transfection, cells on coverslips were transferred to a 0.5-mL bath chamber mounted on the stage of an inverted microscope (Nikon Eclipse) and constantly superfused with external solution kept at 25°C. In patch-clamp experiments with reconstituted Kv4.3 or KCNQ1, only CHO cells that emitted green fluorescence were chosen for current recording. KCNE5 (WT or variant) protein expression was detected by polystyrene microbeads precoated with anti-CD8 antibody (Dynabeads M450; Dynal; Oslo, Norway). Kv4.3 (I_{to}) currents were elicited from a holding potential of −80 mV by 300-ms depolarizing voltage commands. Current amplitudes were measured as the difference between the levels of peak current and that at the end of depolarizing pulse. The time course of Kv4.3 current inactivation was evaluated by fitting the declining phase of the current trace with a double-exponential function as follows (Equation 1):

$$I_{Kv4.3} = A_f \exp(-t/\tau_f) + A_s \exp(-t/\tau_s)$$

where A_f and A_s represent amplitudes, and τ_f and τ_s represent time constants for the fast and slow components, respectively. Voltage dependence of Kv4.3 current activation was studied by constructing mean conductance/voltage (*G*/*V*) relations. The value of *G* for every voltage was calculated from the following expression (Equation 2):

$$G = I/(V - V_{rev})$$

where *I* is Kv4.3 the current amplitude, and V_{rev} is the reversal potential for K^+.

The steady-state activation/inactivation kinetics were fitted to the following Boltzmann equation as follows (Equation 3):

$$Y(V) = 1/(1 + \exp[(V_{1/2} - V)/k])$$

where $V_{1/2}$ is the potential for half-maximal inactivation and activation, respectively; *k* is the slope factor; and *Y* is the normalized conductance or current.

Recovery from inactivation of Kv4.3 current was assessed by a standard paired-pulse protocol as follows: A 500-ms test pulse to +30 mV (P_1) was followed by a variable recovery interval (1 to 600 ms) at −80 mV then by a second 300-ms test pulse to +30 mV (P_2). The time-constant for recovery from inactivation was determined by fitting the mean values of the relation P_2/P_1 versus recovery time to a single exponential function, as follows (Equation 4):

$$P_2/P_1 = A \exp(-t/\tau)$$

where P_2/P_1 is the ratio between Kv4.3 current amplitudes elicited by P_2 and P_1, respectively; *t* is the interpulse interval; *A* is constant; and τ is the recovery time constant.

KCNQ1/KCNE1 currents were evoked by various depolarizing voltage steps with a duration of 2 seconds from holding potential of −80 mV, and tail currents were recorded at −50 mV. Voltage dependence of KCNQ1/KCNE1 activation and inactivation was evaluated by fitting the mean current-voltage (*I*−*V*) relationship of tail currents to the Boltzmann equation (Equation 3).
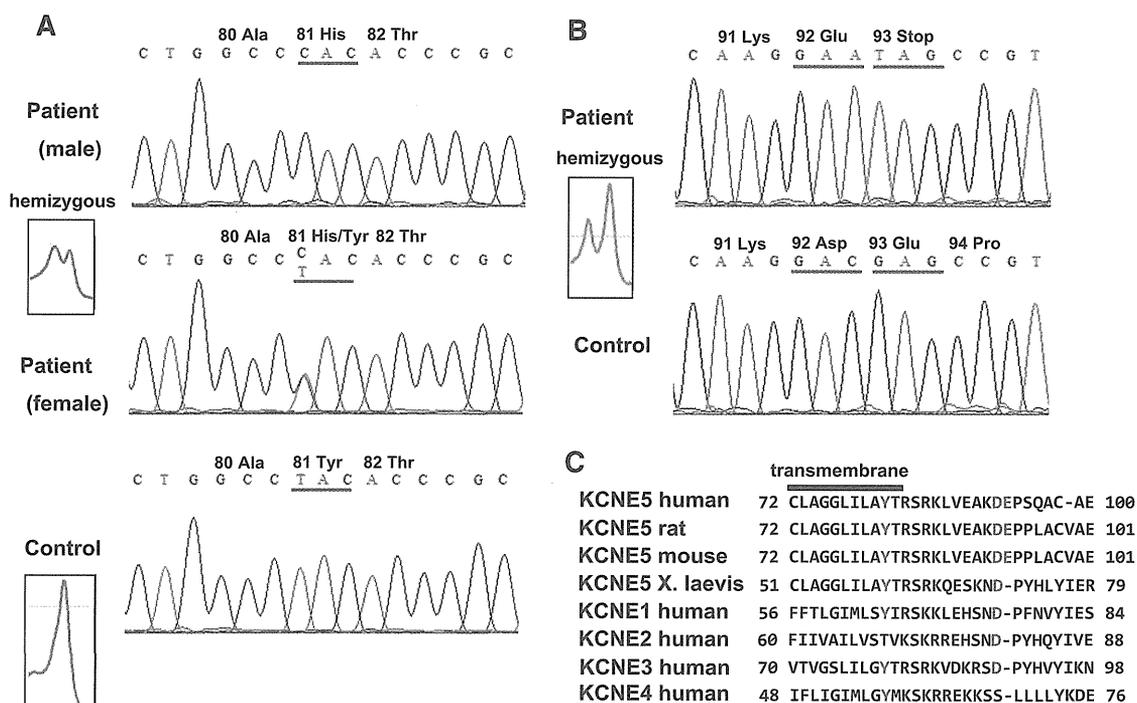
A

80 Ala　81 His　82 Thr
C T G G C C C A C A C C C G C

Patient
(male)
hemizygous

80 Ala　81 His/Tyr　82 Thr
C T G G C C C/T A C A C C C G C

Patient
(female)

80 Ala　81 Tyr　82 Thr
C T G G C C T A C A C C C G C

Control

B

91 Lys　92 Glu　93 Stop
C A A G G A A T A G C C G T

Patient
hemizygous

91 Lys　92 Asp　93 Glu　94 Pro
C A A G G A C G A G C C G T

Control

C

		transmembrane	
KCNE5 human	72	CLAGGLILAYTRSRKLVEAKDEPSQAC-AE	100
KCNE5 rat	72	CLAGGLILAYTRSRKLVEAKDEPPLACVAE	101
KCNE5 mouse	72	CLAGGLILAYTRSRKLVEAKDEPPLACVAE	101
KCNE5 X. laevis	51	CLAGGLILAYTRSRKQESKND-PYHLYIER	79
KCNE1 human	56	FFTLGIMLSYIRSKKLEHSND-PFNVYIES	84
KCNE2 human	60	FIIVAILVSTVKSKRREHSND-PYHQYIVE	88
KCNE3 human	70	VTVGSLILGYTRSRKVDKRSD-PYHVYIKN	98
KCNE4 human	48	IFLIGIMLGYMKSKRREKKSS-LLLLYKDE	76

Figure 1. Molecular discovery of *KCNE5* mutations. Denaturing high-performance liquid chromatography and DNA sequence analyses of control and patients are shown. Abnormal denaturing high-performance liquid chromatography data (inside the frame) was acquired from the mixed sample of a patient and control. **A,** Analyses of patients 1, 2, and 3. DNA sequencing chromatograms demonstrate a Tyr-to-His substitution at residue 81. **B,** Analyses of patient 4. DNA sequencing chromatograms demonstrate an Asp-to-Glu substitution at residue 92 and a Glu-to-stop codon at residue 93. **C,** Alignment of amino acid sequence of KCNE5 in various species and comparison with human KCNE1–4. Red font indicates variant sites and homologies. Asp indicates aspartate; Glu, glutamate; His, histidine; Tyr, tyrosine.

CHO cell membrane capacitance (C_m) was calculated on the basis of the capacitive transients during 20-ms voltage-clamp steps (± 5 mV), using the following equation:

$$C_m = \tau_C\, I_0/\Delta V_m(1-I_{ss}/I_0)$$

where τ_C is the time constant of the capacitive transient, I_0 is the initial peak current amplitude, I_{ss} is the steady-state current value, and ΔV_m is the amplitude of the voltage step (5 mV).

All data are expressed as mean±SEM. Statistical differences between 2 groups of numeric data were determined by unpaired Student t test and 1-way ANOVA followed by Dunnett post hoc analysis in the case of multiple comparisons. $P<0.05$ was considered statistically significant.

Computer Simulation

The dynamic Luo-Rudy model (Clancy and Rudy 2001 model)[22] of a ventricular cell was used with recent modifications. Epicardial and endocardial APs were simulated using a previously reported model. The ratio of I_{Kr} and I_{Ks} conductance of each layer was set as previously reported.[23,24] Maximum conductance in endocardial and epicardial layers was set at 0.05 and 1.1 mS/μF. Electrophysiological alterations caused by 2 mutants were experimentally obtained and incorporated into the model. The maximum conductance of I_{to} was increased by 58% and 80% in the male sex with Y81H and D92E;E93X, respectively. Myocardium models were simulated at the cycle length of 400 ms for 5 minutes.[25]

Results

In 4 of 205 index patients, we identified 2 novel variants in *KCNE5* (Figure 1). The first variant was a single-nucleotide

alternation (c.241T>C) (Figure 1A), resulting in an amino acid substitution from a tyrosine at residue 81 with a histidine (p.Y81H). This Y81H variant was identified in 3 probands. The second variant was found in a male proband and had 2 nucleotide changes (c.[276C>A;277G>T]) (Figure 1B), causing an amino acid substitution from an aspartate at residue 92 with a glutamate and from a glutamate at residue 93 with a stop codon (p.[D92E;E93X]). They are located in the transmembrane (Y81H) and C-terminus (D92E;E93X) and in highly conserved regions (Figure 1C). In 300 unrelated healthy individuals with normal ECGs from the general Japanese population, Y81H was identified in 3 healthy women, and D92E;E93X was absent.

Phenotypic Characterization

Patient 1

The first proband with Y81H was a 41-year-old man who lost consciousness for a few minutes after suffering a convulsion while drinking alcohol. Although he was conscious in the ambulance, he lost consciousness in the hospital emergency department. The monitor ECG at that time displayed VF, and DC shock was performed. His ECGs (Figure 2A) displayed type 1 Brugada pattern, and he received an implantable cardioverter-defibrillator. There was no family history of syncope or sudden cardiac death. The patient's older sister carried the same mutation, but she was healthy and had no
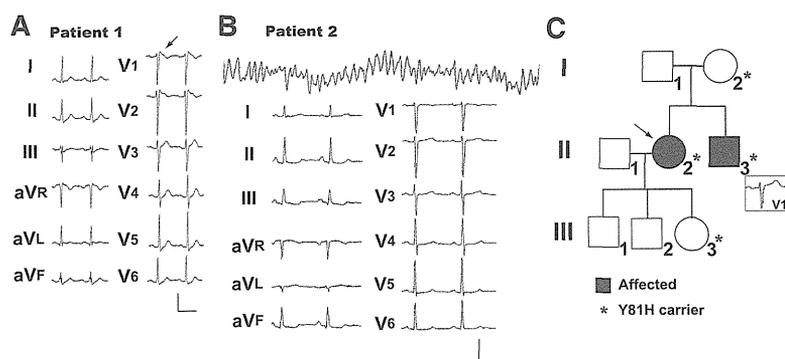
Figure 2. Clinical characterizations of patients with Y81H variant. **A,** Twelve-lead ECG of patient 1. Arrow indicates coved-type ST-segment elevation. **B,** ECG recording of patient 2. Top shows ventricular fibrillation recorded in automatic electric defibrillation, and bottom shows a 12-lead ECG for patient 2. Bars indicate 1 mV and 400 ms. **C,** Family tree of patient 2. Patient 2 (proband) is indicated by arrow (II-2). Roman numerals refer to the different generations, and numbers 1 through 3 identify individuals within each generation. Circles indicate female family members and squares, male family members. The affected family members are filled, and Y81H carriers are indicated with an asterisk. V_1 lead recording in the inset is of II-3.

history of syncope. Her ECG did not show Brugada pattern (not shown).

Patient 2

The second proband with Y81H was a 47-year-old women who fell down suddenly while working at the cash desk of a supermarket. She immediately underwent cardiopulmonary resuscitation and was transported to the hospital. The recording of automatic external defibrillation showed VF (Figure 2B, top). Although there was no sign of ischemic heart disease through cardiac angiography examination, VF was induced during electrophysiological examination. The patient received an implantable cardioverter-defibrillator. Her ECG showed no ST elevation in the right precordial leads (Figure 2B, bottom) and did not show Brugada pattern for the next follow-up period. In the flecainide infusion test, ST-segment elevation in the right precordial leads was not produced. Figure 2C shows the patient's family tree. Her younger brother (II-3) had a history of syncope and carried the same mutation, although his ECG did not show Brugada pattern (Figure 2C inset), even in the superior-costal position. His ECG also showed no conduction or depolarizing disturbance

(PR, 170 ms; QRS, 100 ms; QT, 388 ms; QTc, 433 ms). The patient's mother (I-2) and daughter (III-3) were carrying the same mutation but remain asymptomatic and showed no Brugada pattern on ECG.

Patient 3

The third proband with Y81H was a 54-year-old woman who had syncope when she was drinking alcohol and watching television. After a few minutes, she recovered consciousness. Her ECG showed ST elevation in the V_1 and V_2 leads recorded a few days after the event (data not shown); therefore, cardiac electrophysiology testing was performed. In the test, VF could be induced, and the patient received an implantable cardioverter-defibrillator. The patient had no family history of syncope and sudden cardiac death. Her relatives did not give consent for genetic analysis.

Patient 4

A novel variant, D92E;E93X, was identified in a 59-year-old man who was a postal worker. When he started a ride on his motorcycle after a postal delivery, he suddenly lost consciousness. He recovered consciousness in the ambulance. At
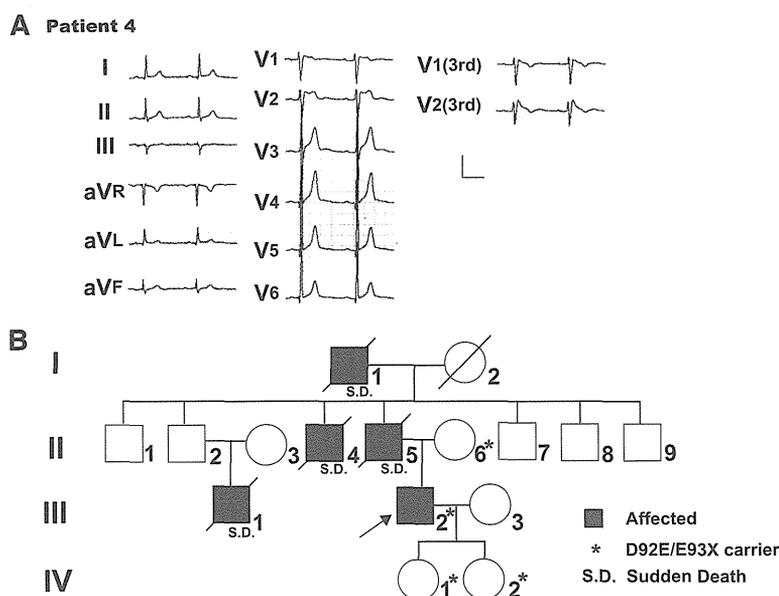

Figure 3. Clinical characterizations of patient 4. **A,** Twelve-lead ECG of patient 4. Right-side ECGs (3rd) were recorded in third costal position. Bars indicate 1 mV and 400 ms. **B,** Family tree of patient 4. Patient 4 (proband) is indicated by an arrow (III-2). Roman numerals refer to the different generations, and numbers 1 through 9 identify individuals within each generation. Circles indicate female family members and squares, male family members. Slashes indicate deceased family members, and S.D. indicates individuals who died suddenly. The affected family members are filled and D92E;E93X carriers are indicated with an asterisk.
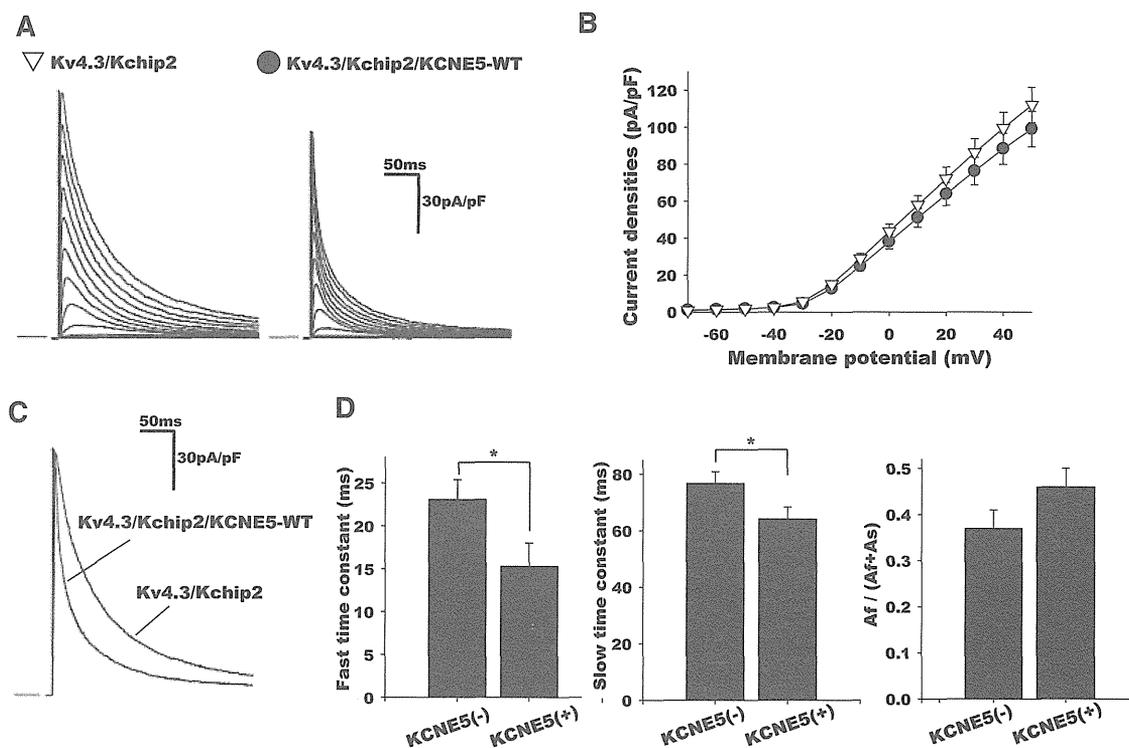
Figure 4. Functional analysis of *KCNE5* on Kv4.3/Kv channel-interacting protein (KChIP2) current. **A,** Representative Kv4.3/KChIP2 current traces without or with *KCNE5*. Cells were held at −80 mV and stepped to various test potentials ranging from −70 to +50 mV in 10-mV steps for 300 ms. Scale bars indicate 50 ms and 30 pA/pF. **B,** Current voltage relationships are as follows: ▽ without KCNE5 (n=15), ● with KCNE5 (n=19). **C,** Representative KV4.3/KChIP2 current traces with or without KCNE5 elicited by +50 mV. **D,** Inactivation time constant calculated by fitting a double exponential function (see Equation 1) to tail current after depolarized to +50 mV. *$P<0.05$ versus WT. pA/pF indicates picoamperes per picofarad; WT, wild type.

that time, he had a fever and his body temperature was 38.0°C. His ECG (Figure 3A) showed saddle-back-type ST elevation in the right precordial leads and coved-type ST elevation at the third costal position. We therefore diagnosed symptomatic BrS, and the patient received an implantable cardioverter-defibrillator. The patient's grandfather (I-1), father (II-5), uncle (II-4), and paternal cousin (III-1) all died suddenly at the ages of 45, 52, 45, and 31, respectively (Figure 3B). In genetic analysis, his mother and 2 daughters carried this mutation in a heterozygous manner; however, all were asymptomatic and had no Brugada pattern on ECG.

Four probands tested negative for the causative genes of BrS as described in the Methods. Also, they were negative for the reported Ca channel mutations.

Electrophysiological Analysis

Effects of KCNE5 on Kv4.3/KChIP2 Current Amplitude and Kinetics

To examine the effects of the *KCNE5* variants on I_{to}, we first coexpressed the *KCND3* gene product (Kv4.3, the α-subunit of I_{to} channel) and *KChIP2* (the principle β-subunit for human native cardiac I_{to}[15,26,27]) in CHO cells. Figure 4A shows representative whole-cell current traces recorded from cells cotransfected with *KCND3*, *KChIP2*, and without (left) or with (right) *KCNE5*. Cells expressing Kv4.3/KChIP2

channels alone showed rapidly activating and inactivating currents. Coexpression of *KCNE5* reduced peak current densities as summarized in Figure 4B but not to a statistically significant extent. Figure 4C shows 2 current traces recorded from cells cotransfected with or without *KCNE5*. Two peak levels were adjusted to show the time course of inactivation. This was significantly more rapid in the presence of *KCNE5* ($P<0.05$), as shown by the plots of inactivation time constants (obtained using Equation 1) shown in Figure 4D.

KCNE5 Variants Increase Kv4.3/KChIP2 Current

We then examined the functional effect of 2 novel *KCNE5* variants on Kv4.3/KChIP2 currents. The 5 parts of Figure 5A show current traces elicited by depolarizing pulses from a holding potential of −80 mV in cells cotransfected with KCNE5-WT, Y81H, D92E;E93X, Y81H+WT, and D92E;E93X+WT. Both *KCNE5* variants significantly increased Kv4.3/KChIP2 currents (○ and ▼). However, when cotransfected with WT and respective variants at a 1:1 ratio, this stimulatory action of *KCNE5* variants was completely abolished (◆ and □). Figure 5B summarizes peak current-membrane potential relations. Each symbol indicates the mean current density calculated from pooled data at respective test potentials, and vertical bars indicate SEs. With a depolarization to +50 mV, for example, the current densities
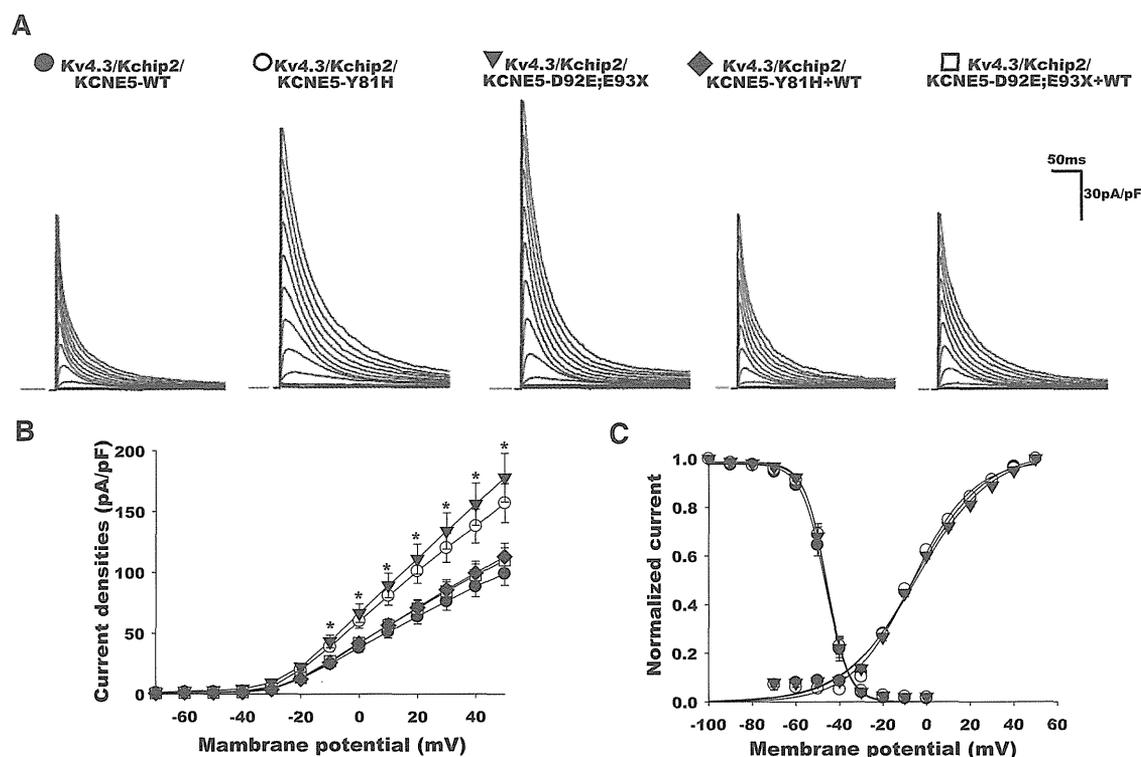
Figure 5. Functional analysis of *KCNE5* variants on Kv4.3/KChIP2 current. **A**, Representative Kv4.3/KChIP2 current traces with KCNE5-WT or variants. Cells were held at −80 mV and stepped to various test potentials ranging from −70 to +50 mV in 10-mV steps for 300 ms. Scale bars indicate 50 ms and 30 pA/pF. **B**, Current voltage relationships are as follows: ● with KCNE5-WT (n=19), ○ with KCNE5–Y81H (n=22), ▼ with KCNE5–D92E;E93X (n=20), ◆ with KCNE5–Y81H+WT (n=18), and □ with KCNE5–D92E;E93X+WT (n=27). *P<0.05 versus WT. **C**, Normalized activation and inactivation current of Kv4.3/KChIP2/KCNE5 fitted to Boltzmann equation (Equation 3). To see the current inactivation, cells were depolarized from −100 to 0 mV in 10-mV increments for 1 second, then depolarized to 30 mV for 300 ms and returned to −80-mV holding potential. Abbreviations as in Figure 4.

were 98.9±9.9 picoamperes per picofarad (pA/pF), 156.5±15.9 pA/pF, and 178.0±20.0 pA/pF in the presence of KCNE5-WT (n=19), Y81H (n=22), and D92E;E93X (n=20), respectively (*P*<0.05 versus WT). In contrast, when coexpressed with WT and *KCNE5* variants, they were 112.5±11.1 pA/pF and 109.8±10.2 pA/pF for the WT/Y81H (n=18) and WT/D92E;E93X (n=27), respectively (*P*>0.05 versus WT).

Effects of *KCNE5* variants on voltage dependence for Kv4.3/KChIP2 currents were studied in terms of current activation/inactivation (Figure 5C, Table 1). The values of $V_{1/2}$ and k for KCNE5-WT were not statistically different

from those for variant KCNE5 proteins, thus indicating that variants did not affect either activation or inactivation kinetics of Kv4.3/KChIP2 currents.

Inactivation time courses also were assessed using Equation 1 and are summarized in Figure 6A and Table 1. The fast time constant for inactivation (τ_f) was 15.3±2.7 ms, 24.5±2.4 ms, and 14.7±2.2 ms; the slow time constant (τ_s) was 64.2±4.2 ms, 63.8±4.0 ms, and 57.1±2.1 ms; and the fraction of the amplitude of the fast inactivation component was 0.46±0.04, 0.38±0.04, and 0.42±0.02 for WT (n=18), Y81H (n=18), and D92E;E93X (n=21), respectively. The value of τ_f for Y81H (but not D92E;E93X) was significantly

Table 1. Electrophysiological Analysis of I_{to}

	Peak Current Density at +50 mV, pA/pF	Activation		Inactivation		Inactivation Time Constant (τ)			Recovery of Inactivation, ms
		$V_{1/2}$, mV	Slope Factor, κ	$V_{1/2}$, mV	Slope Factor, κ	Fast (τ_f), ms	Slow (τ_s), ms	$A_f/(A_f+A_s)$	
WT	98.9±9.9	−2.0±2.0	18.2±1.9	−46.2±1.2	−4.2±0.1	15.3±2.7	64.2±4.2	0.46±0.04	47.1±4.5
Y81H	156.5±15.9*	−5.7±0.9	14.2±0.6	−45.8±0.9	−4.5±0.1	24.5±2.4*	63.8±4.0	0.38±0.04	50.0±5.4
D92E;E93X	178.0±20.0*	−3.5±1.3	16.6±1.3	−45.9±0.9	−4.4±0.1	14.7±2.2	57.1±2.1	0.42±0.02	41.9±4.5

Data are presented as mean±SEM. *A* indicates amplitude; I_{to}, transient outward current; pA/pF, picoamperes per picofarad; $V_{1/2}$, potential for half-maximal inactivation and activation; WT, wild type.
  *P<0.05 vs WT.
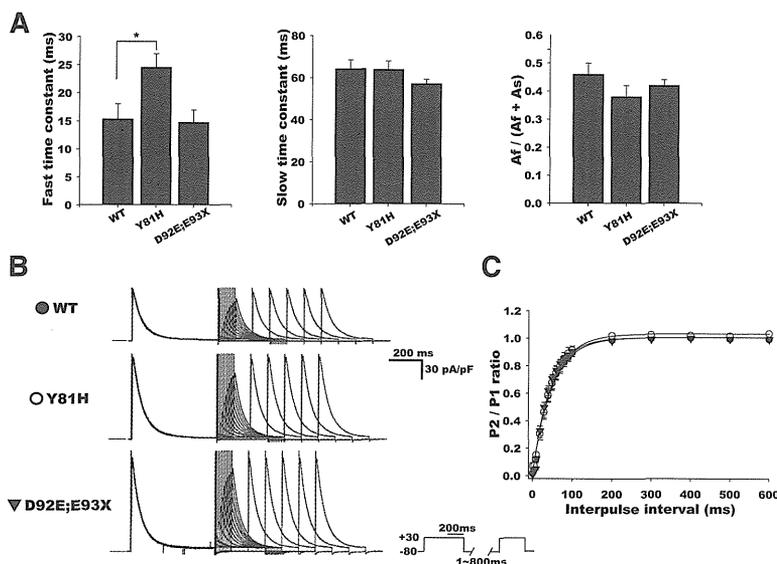
A

B

● WT

○ Y81H

▽ D92E;E93X

C

Figure 6. Inactivation kinetics and recovery from inactivation of Kv4.3/KChIP2/KCNE5 current. **A**, Inactivation time constant calculated by fitting a double exponential function (Equation 1) to tail current after depolarized to $+50$ mV. $^*P<0.05$ versus WT. **B**, Representative current traces illustrating recovery from inactivation. Recovery from inactivation was assessed by a 2-pulse protocol (inset) as follows: a 400-ms test pulse to $+30$ mV (P_1) followed by a variable interval at -80 mV and then by a second test pulse to $+30$ mV (P_2). **C**, Mean value of P_2/P_1 ratio plotted as a function of interpulse interval and fitted to Equation 4. Abbreviations as in Figure 4.

larger than that for WT. There were no significant differences between the values of τ_s or the fraction of fast inactivating current for WT and variant *KCNE5*.

In the next series of experiments, a 2-pulse protocol was used to investigate the recovery of inactivation of Kv4.3/KChIP2 currents in CHO cells (see Methods section). Figure 6B shows typical examples of time-dependent recovery of the Kv4.3/KChIP2 current amplitudes when WT or variant *KCNE5* was coexpressed. In Figure 6C, the mean P_2/P_1 ratios are plotted as a function of interpulse interval and are fitted to Equation 4. The time constants for recovery of inactivation thus calculated were not significantly different, suggesting that 2 variants did not affect the recovery of Kv4.3/KChIP2 channel activity from inactivation (Table 1).

KCNE5 *Mutants and KCNQ1+KCNE1 Channel*
Recently, novel mutation in a conserved residue of KCNQ1 (gene coding α-subunit of the KCNQ1+KCNE1 [I_{Ks}] channel), V162M, was reported to cause BrS by accelerating current activation.[9] Therefore, we tested the effect of WT and variant *KCNE5* on reconstituted I_{Ks} current in CHO cells. Figure 7A shows representative current traces of I_{Ks} with or without *KCNE5*. As previously reported,[28] cotransfection of WT *KCNE5* reduced I_{Ks} without changing activation gating kinetics. Numeric data obtained from pooled experiments are summarized in Table 2. Two *KCNE5* variants exerted effects analogous to WT *KCNE5* on I_{Ks} currents, reducing them without changing the activation gate kinetics, and there was no statistical difference between WT and the 2 mutants.

Finally, deactivation time constants for tail currents were calculated by fitting a single exponential equation and are summarized in Table 2. They were not significantly different, suggesting that the 2 *KCNE5* variants did not affect I_{Ks} channel function in a way different from that of WT *KCNE5*.

Simulation Study
AP simulations were conducted to determine the effects of the *KCNE5* variants on ventricular AP profiles. Figure 8

shows representative results. Simulated APs from epicardial and endocardial layers are overlapped. Compared to WT (Figure 8A), the myocardium model with Y81H (Figure 8B) demonstrated a notch-and-dome AP morphology and loss-of-
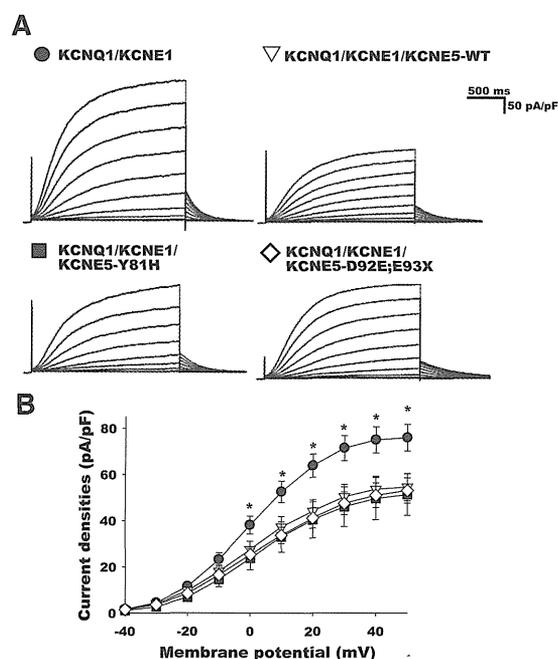
A

B

Figure 7. Functional analysis of *KCNE5* variants on KCNQ1/KCNE1 current. **A**, Representative KCNQ1/KCNE1 current traces without or with KCNE5-WT or variants. Cells were held at -80 mV and stepped to various test potentials ranging from -40 to $+50$ mV in 10-mV steps for 2 seconds and subsequent repolarization to -50 mV. Scale bars indicate 500 ms and 50 pA/pF. **B**, Current voltage relationships are as follows: ● without KCNE5 ($n=14$), ▽ with KCNE5-WT ($n=21$), ■ with KCNE5-Y81H ($n=6$), and ◇ with KCNE5–D92E;E93X ($n=8$). $^*P<0.05$ versus *KCNE5*. Abbreviation as in Figure 4.

Table 2. Electrophysiological Analysis of I_{Ks}

	Tail Current Density at +50 mV, pA/pF	Activation	
		$V_{1/2}$, mV	Slope Factor, κ
Q1/E1	76.0±5.7	0.7±1.6	11.5±0.4
Q1/E1/E5WT	54.6±5.9	1.9±1.4	12.7±0.4
Q1/E1/E5Y81H	51.2±8.9	3.7±2.0	13.0±0.6
Q1/E1/E5D92E;E93X	53.0±5.4	2.6±2.2	13.6±0.3

Data are presented as mean±SEM. I_{Ks} indicates KCNQ1+KCNE1 channel. Other abbreviations as in Table 1.

dome pattern similar in the simulation study with Na channel mutation.[23] The model with D92E;E93X showed a loss-of-dome pattern (Figure 8C). These patterns would be anticipated to lead to larger voltage gradients in the ventricular transmural models, increasing the likelihood of a proarrhythmic substrate.

Discussion

In the present study, we identified 2 novel variants in *KCNE5* (*KCNE1L*) in patients with BrS or IVF and demonstrated that these variants upregulated reconstituted I_{to} compared with WT *KCNE5*. *KCNE5* was first reported as *KCNE1*-like gene because of homology with KCNE1,[16] coding a single-transmembrane-domain protein. As a member of *KCNE* family (1 through 5), it can function as an ancillary subunit of Kv channels. Recently, a *KCNE5* mutation, L65F, was found to be associated with AF.[29] WT *KCNE5* suppresses I_{Ks},[30] but

Figure 8. Simulation study of KCNE5-WT and mutants. **A**, WT models. Gray lines indicate the action potential in epicardium, and black indicates action potential endocardium. **B**, Y81H model displays notch-and-dome and loss-of-dome pattern in epicardium. **C**, D92E;E93X model displays loss-of-dome pattern in epicardium.

the L65F mutation failed to suppress I_{Ks}, therefore exerting a gain of function effect on I_{Ks} and predisposing to atrial fibrillation.

In the present functional assay of 2 novel *KCNE5* variants, Y81H and D92E;E93X (Figure 5), the coexpression of variant with WT *KCNE5* subunits (to mimic the heterozygous condition) abolished the stimulatory action of the mutants. Given that *KCNE5* is located in the X chromosome, the upregulation of I_{to} currents may occur preferentially in male (XY) than in female mutation carriers (XX). In other words, the male sex would be anticipated to have more lethal phenotypes than the female sex. Indeed, we identified 11 mutant carriers in the 4 families; 3 men and 8 women. All the male cases were symptomatic, and 2 of them showed a typical Brugada pattern on ECG, whereas 6 of 8 female cases remained asymptomatic. Interestingly, all the female carriers, including 2 symptomatic probands, did not show typical Brugada patterns on ECG. In total, only 2 men among 11 carriers had a Brugada pattern on ECG, and both developed VF. This sex difference in ECG features also may partially result from the sex-dependent difference in I_{to} current density.[31]

In 300 controls, we identified 3 female heterozygous Y81H carriers but no D92E;E93X carriers. Both cases (obligatory heterozygous because they are female [XX]) showed normal ECG and were asymptomatic. Y81H-KCNE5, therefore, could be a genetic polymorphism but not a mutation; however, the functional assay of both variants showed that they cause a larger I_{to} in case of male carriers (XY), which would be expected to influence transmural dispersion of repolarization and, thereby, arrhythmogenicity. It remains unknown why 2 female Y81H-KCNE5 carriers were symptomatic because they have 2 X chromosomes. However, X chromosome inactivation may be related to this phenomenon[32] because it results in the random silencing of 1 of the paired X chromosomes in mammalian females to achieve the dosage equivalency with males. Once an X is to be active or inactive during late blastocyst stage, this state is stably inherited through subsequent somatic miotic divisions, resulting in females being mosaics for cells with each parental X active. Recently, Carrel and Willard[33] reported that ≈15% of X-linked genes escape from the inactivation phenomenon to some degree, therefore explaining the expression heterogeneity among the female sex. In our 2 female cases with symptomatic VF, similar mechanisms, such as gene inactivation and its escape phenomenon, may underlie the arrhythmogeneity by causing diverse levels of mutant *KCNE5* expression. This in turn may change the densities and properties of resultant I_{to} currents.

In contrast, D92E;E93X-KCNE5 identified in the family of patient 4 (Figure 3) appeared to serve as a genetic modifier because sudden death accumulated in the proband's paternal side (Figure 3B, pedigree). D92E;E93X was inherited from his mother and then transferred to his 2 daughters. Therefore, we could not completely exclude the possibility of the presence of another genetic background predisposing to IVF, which was inherited from his father's side, although he tested negative for previously reported candidate genes for BrS. Our experimental study implicated that his 2 daughters are at a
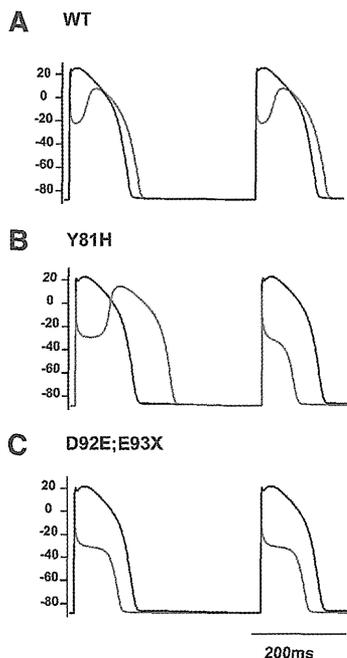
higher risk of IVF and have a potential to transmit the arrhythmogenicity to their offspring, especially male ones. These poor genotype-phenotype correlations indicate that these *KCNE5* variants do not confer final causality but are more likely to modulate the electrocardiographic and arrhythmic manifestations of BrS or IVF secondary to other causes.

With regard to candidate genes responsible for BrS or IVF, Kv4.3, encoded by *KCND3* and an α-subunit for the I_{to} channel, has been believed plausible to cause transmural repolarization dispersion and arrhythmogeneity.[34] However, there are no reports on *KCND3* mutations in patients with these pathological conditions. More recently, a mutation of *KCNE3* (R99H), another β-subunit for voltage-gated K channels, was found in a BrS family and has been shown to increase I_{to} current and accelerate its inactivation by interacting with Kv4.3 and KChIP2.[8] The 2 *KCNE5* mutations described in the present study increased I_{to}. Thus, *KCNE5* variants appear to be modifiers of phenotype and arrhythmogeneity. Screening for *KCNE5* mutations may help to detect patients at risk for sudden cardiac death.

Disclosures
None.

References
1. Brugada P, Brugada J. Right bundle branch block, persistent ST segment elevation and sudden cardiac death: a distinct clinical and electrocardiographic syndrome. A multicenter report. *J Am Coll Cardiol*. 1992;20:1391–1396.
2. Benito B, Sarkozy A, Mont L, Henkens S, Berruezo A, Tamborero D, Arzamendi D, Berne P, Brugada R, Brugada P, Brugada J. Gender differences in clinical manifestations of Brugada syndrome. *J Am Coll Cardiol*. 2008;52:1567–1573.
3. Chen Q, Kirsch GE, Zhang D, Brugada R, Brugada J, Brugada P, Potenza D, Moya A, Borggrefe M, Breithardt G, Ortiz-Lopez R, Wang Z, Antzelevitch C, O'Brien RE, Schulze-Bahr E, Keating MT, Towbin JA, Wang Q. Genetic basis and molecular mechanism for idiopathic ventricular fibrillation. *Nature*. 1998;392:293–296.
4. Antzelevitch C, Brugada P, Borggrefe M, Brugada J, Brugada R, Corrado D, Gussak I, LeMarec H, Nademanee K, Perez Riera AR, Shimizu W, Schulze-Bahr E, Tan H, Wilde A. Brugada syndrome: report of the second consensus conference: endorsed by the Heart Rhythm Society and the European Heart Rhythm Association. *Circulation*. 2005;111:659–670.
5. London B, Michalec M, Mehdi H, Zhu X, Kerchner L, Sanyal S, Viswanathan PC, Pfahnl AE, Shang LL, Madhusudanan M, Baty CJ, Lagana S, Aleong R, Gutmann R, Ackerman MJ, McNamara DM, Weiss R, Dudley SC Jr. Mutation in glycerol-3-phosphate dehydrogenase 1 like gene (GPD1-L) decreases cardiac Na$^+$ Current and causes inherited arrhythmias. *Circulation*. 2007;116:2260–2268.
6. Antzelevitch C, Pollevick GD, Cordeiro JM, Casis O, Sanguinetti MC, Aizawa Y, Guerchicoff A, Pfeiffer R, Oliva A, Wollnik B, Gelber P, Bonaros EP Jr, Burashnikov E, Wu Y, Sargent JD, Schickel S, Oberheiden R, Bhatia A, Hsu LF, Haissaguerre M, Schimpf R, Borggrefe M, Wolpert C. Loss-of-function mutations in the cardiac calcium channel underlie a new clinical entity characterized by ST-segment elevation, short QT intervals, and sudden cardiac death. *Circulation*. 2007;115:442–449.
7. Watanabe H, Koopmann TT, Le Scouarnec S, Yang T, Ingram CR, Schott JJ, Demolombe S, Probst V, Anselme F, Escande D, Wiesfeld AC, Pfeufer A, Kaab S, Wichmann HE, Hasdemir C, Aizawa Y, Wilde AA, Roden DM, Bezzina CR. Sodium channel $\beta1$ subunit mutations associated with Brugada syndrome and cardiac conduction disease in humans. *J Clin Invest*. 2008;118:2260–2268.
8. Delpon E, Cordeiro JM, Nunez L, Thomsen PE, Guerchicoff A, Pollevick GD, Wu Y, Kanters JK, Larsen CT, Burashnikov E, Christiansen M, Antzelevitch C. Functional effects of KCNE3 mutation and its role in the development of Brugada syndrome. *Circ Arrhythm Electrophysiol*. 2008;1:209–218.
9. Barajas-Martinez H, Hu D, Burashnikov E, Antzelevitch C. Novel mutation in the KCNQ1 associated with Brugada syndrome. *Circulation*. 2008;118:S332.
10. Makiyama T, Akao M, Tsuji K, Doi T, Ohno S, Takenaka K, Kobori A, Ninomiya T, Yoshida H, Takano M, Makita N, Yanagisawa F, Higashi Y, Takeyama Y, Kita T, Horie M. High risk for bradyarrhythmic complications in patients with Brugada syndrome caused by SCN5A gene mutations. *J Am Coll Cardiol*. 2005;46:2100–2106.
11. Makiyama T, Akao M, Haruna Y, Tsuji K, Doi T, Ohno S, Nishio Y, Kita T, Horie M. Mutation analysis of the glycerol-3 phosphate dehydrogenase-1 like (GPD1L) gene in Japanese patients with Brugada syndrome. *Circ J*. 2008;72:1705–1706.
12. Yan GX, Antzelevitch C. Cellular basis for the Brugada syndrome and other mechanisms of arrhythmogenesis associated with ST-segment elevation. *Circulation*. 1999;100:1660–1666.
13. Calloe K, Cordeiro JM, Di Diego JM, Hansen RS, Grunnet M, Olesen SP, Antzelevitch C. A transient outward potassium current activator recapitulates the electrocardiographic manifestations of Brugada syndrome. *Cardiovasc Res*. 2009;81:686–694.
14. Patel SP, Campbell DL. Transient outward potassium current, 'Ito,' phenotypes in the mammalian left ventricle: underlying molecular, cellular and biophysical mechanisms. *J Physiol*. 2005;569(pt 1):7–39.
15. Radicke S, Cotella D, Graf EM, Banse U, Jost N, Varro A, Tseng GN, Ravens U, Wettwer E. Functional modulation of the transient outward current I_{to} by KCNE β-subunits and regional distribution in human non-failing and failing hearts. *Cardiovasc Res*. 2006;71:695–703.
16. Piccini M, Vitelli F, Seri M, Galietta LJ, Moran O, Bulfone A, Banfi S, Pober B, Renieri A. KCNE1-like gene is deleted in AMME contiguous gene syndrome: identification and characterization of the human and mouse homologs. *Genomics*. 1999;60:251–257.
17. Ravn LS, Hofman-Bang J, Dixen U, Larsen SO, Jensen G, Haunso S, Svendsen JH, Christiansen M. Relation of 97T polymorphism in KCNE5 to risk of atrial fibrillation. *Am J Cardiol*. 2005;96:405–407.
18. Ohno S, Zankov DP, Yoshida H, Tsuji K, Makiyama T, Itoh H, Akao M, Hancox JC, Kita T, Horie M. N- and C-terminal KCNE1 mutations cause distinct phenotypes of long QT syndrome. *Heart Rhythm*. 2007;4:332–340.
19. Hofman-Bang J, Jespersen T, Grunnet M, Larsen LA, Andersen PS, Kanters JK, Kjeldsen K, Christiansen M. Does KCNE5 play a role in long QT syndrome? *Clin Chim Acta*. 2004;345:49–53.
20. Ohno S, Toyoda F, Zankov DP, Yoshida H, Makiyama T, Tsuji K, Honda T, Obayashi K, Ueyama H, Shimizu W, Miyamoto Y, Kamakura S, Matsuura H, Kita T, Horie M. Novel KCNE3 mutation reduces repolarizing potassium current and associated with long QT syndrome. *Hum Mutat*. 2009;30:557–563.
21. Kubota T, Shimizu W, Kamakura S, Horie M. Hypokalemia-induced long QT syndrome with an underlying novel missense mutation in S4–S5 linker of KCNQ1. *J Cardiovasc Electrophysiol*. 2000;11:1048–1054.
22. Clancy CE, Rudy Y. Cellular consequences of HERG mutations in the long QT syndrome: precursors to sudden cardiac death. *Cardiovasc Res*. 2001;50:301–313.
23. Clancy CE, Rudy Y. Na$^+$ channel mutation that causes both Brugada and long-QT syndrome phenotypes: a simulation study of mechanism. *Circulation*. 2002;105:1208–1213.
24. Liu DW, Gintant GA, Antzelevitch C. Ionic bases for electrophysiological distinctions among epicardial, midmyocardial, and endocardial myocytes from the free wall of the canine left ventricle. *Circ Res*. 1993;72:671–687.
25. Itoh H, Sakaguchi T, Ding WG, Watanabe E, Watanabe I, Nishio Y, Makiyama T, Ohno S, Akao M, Higashi Y, Zenda N, Kubota T, Mori C, Okajima K, Haruna T, Miyamoto A, Kawamura M, Ishida K, Nagaoka I, Oka Y, Nakazawa Y, Yao T, Jo H, Sugimoto Y, Ashihara T, Hayashi H, Ito M, Imoto K, Matsuura H, Horie M. Latent genetic backgrounds and

molecular pathogenesis in drug-induced long-QT syndrome. *Circ Arrhythm Electrophysiol.* 2009;2:511–523.

26. An WF, Bowlby MR, Betty M, Cao J, Ling HP, Mendoza G, Hinson JW, Mattsson KI, Strassle BW, Trimmer JS, Rhodes KJ. Modulation of A-type potassium channels by a family of calcium sensors. *Nature.* 2000;403:553–556.

27. Decher N, Uyguner O, Scherer CR, Karaman B, Yuksel-Apak M, Busch AE, Steinmeyer K, Wollnik B. hKChIP2 is a functional modifier of hKv4.3 potassium channels: cloning and expression of a short hKChIP2 splice variant. *Cardiovasc Res.* 2001;52:255–264.

28. Lundquist AL, Manderfield LJ, Vanoye CG, Rogers CS, Donahue BS, Chang PA, Drinkwater DC, Murray KT, George AL Jr. Expression of multiple KCNE genes in human heart may enable variable modulation of I_{Ks}. *J Mol Cell Cardiol.* 2005;38:277–287.

29. Ravn LS, Aizawa Y, Pollevick GD, Hofman-Bang J, Cordeiro JM, Dixen U, Jensen G, Wu Y, Burashnikov E, Haunso S, Guerchicoff A, Hu D,

Svendsen JH, Christiansen M, Antzelevitch C. Gain of function in I_{Ks} secondary to a mutation in KCNE5 associated with atrial fibrillation. *Heart Rhythm.* 2008;5:427–435.

30. Angelo K, Jespersen T, Grunnet M, Nielsen MS, Klaerke DA, Olesen SP. KCNE5 induces time- and voltage-dependent modulation of the KCNQ1 current. *Biophys J.* 2002;83:1997–2006.

31. Di Diego JM, Cordeiro JM, Goodrow RJ, Fish JM, Zygmunt AC, Perez GJ, Scornik FS, Antzelevitch C. Ionic and cellular basis for the predominance of the Brugada syndrome phenotype in males. *Circulation.* 2002; 106:2004–2011.

32. Lyon MF. Sex chromatin and gene action in the mammalian X-chromosome. *Am J Hum Genet.* 1962;14:135–148.

33. Carrel L, Willard HF. X-inactivation profile reveals extensive variability in X-linked gene expression in females. *Nature.* 2005;434:400–404.

34. Antzelevitch C, Yan GX. Cellular and ionic mechanisms responsible for the Brugada syndrome. *J Electrocardiol.* 2000;33(suppl):33–39.

CLINICAL PERSPECTIVE

Brugada syndrome (BrS) and idiopathic ventricular fibrillation (IVF) are malignant cardiac disorders that cause syncope and sudden death without structural abnormality. Their frequency is much higher in male sex than in female sex, although the reason remains unclear. In electrophysiological analyses, BrS was shown to be associated with reductions in Na or Ca currents or increases in transient outward K^+ current (I_{to}). In light of sex differences, we focused on the *KCNE5* gene because it is located on the X chromosome. In the present cohort of patients with BrS or IVF (N=205), we found 2 novel *KCNE5* variants in 4 symptomatic probands. A similar *KCNE5* variant also was identified in 3 asymptomatic female controls. In patch-clamp analysis using a heterologous expression system, both *KCNE5* variants increased the I_{to} current. In a computer simulation study, both variants demonstrated notch-and-dome or loss-of-dome patterns, which could lead to larger voltage gradients in the ventricular transmural models. Thus, *KCNE5* variants modulate I_{to} current and, thereby, the phenotypes of BrS and IVF more predominantly in male patients. Although further study in a larger cohort of patients with BrS or IVF is needed, *KCNE5* screening in these patients may be useful to predict prognosis.

A Novel *KCNJ2* Nonsense Mutation, S369X, Impedes Trafficking and Causes a Limited Form of Andersen-Tawil Syndrome

Takahiro Doi, MD; Takeru Makiyama, MD, PhD; Takeshi Morimoto, MD, PhD;
Yoshisumi Haruna, MD, PhD; Keiko Tsuji, BSc; Seiko Ohno, MD, PhD; Masaharu Akao, MD, PhD;
Yoshiaki Takahashi, MD, PhD; Takeshi Kimura, MD, PhD; Minoru Horie, MD, PhD

Background—Mutations in *KCNJ2*, a gene encoding the inward rectifier K$^+$ channel Kir2.1, are associated with Andersen-Tawil syndrome (ATS), which is characterized by (1) ventricular tachyarrhythmias associated with QT (QU)-interval prolongation, (2) periodic paralysis, and (3) dysmorphic features.

Methods and Results—We identified a novel *KCNJ2* mutation, S369X, in a 13-year-old boy with prominent QU-interval prolongation and mild periodic paralysis. The mutation results in the truncation at the middle of the cytoplasmic C-terminal domain that eliminates the endoplasmic reticulum (ER)-to-Golgi export signal. Current recordings from Chinese hamster ovary cells transfected with *KCNJ2*-S369X exhibited significantly smaller K$^+$ currents compared with *KCNJ2* wild type (WT) (1 μg each) (-84 ± 14 versus -542 ± 46 picoamperes per picofarad [pA/pF]; -140 mV; $P<0.0001$). Coexpression of the WT and S369X subunits did not show a dominant-negative suppression effect but yielded larger currents than those of WT+S369X (-724 ± 98 pA/pF$>-[84+542]$ pA/pF; 1 μg each; -140 mV). Confocal microscopy analysis showed that the fluorescent protein-tagged S369X subunits were predominantly retained in the ER when expressed alone; however, the expression of S369X subunits to the plasma membrane was partially restored when coexpressed with WT. Fluorescence resonance energy transfer analysis demonstrated direct protein-protein interactions between WT and S369X subunits in the intracellular compartment.

Conclusions—The S369X mutation causes a loss of the ER export motif. However, the trafficking deficiency can be partially rescued by directly assembling with the WT protein, resulting in a limited restoration of plasma membrane localization and channel function. This alleviation may explain why our patient presented with a relatively mild ATS phenotype. (***Circ Cardiovasc Genet***. 2011;4:253-260.)

Key Words: Long QT Syndrome ■ tachyarrhythmias ■ KCNJ2 ■ ion channels ■ mutation

Andersen-Tawil syndrome (ATS) (OMIM [Online Mendelian Inheritance in Man] #170390) is a rare disorder inherited in an autosomal-dominant fashion. ATS is characterized by (1) ventricular tachyarrhythmias associated with a prolongation of QT (QU) on ECG, (2) periodic paralysis, and (3) dysmorphic features.[1–4] The characteristics of ATS vary greatly among patients, with some presenting with all 3 symptoms and others presenting with only 2.[3–7] In 2001, Plaster et al,[5] identified heterozygous mutations in the *KCNJ2* gene (OMIM *600681) encoding the inward rectifying K$^+$ channel Kir2.1 in patients with ATS. The *KCNJ2* gene is located at 17q23, and its open reading frame is not interrupted by introns.[5] The deduced protein sequence comprises 427 amino acids, with 2 putative membrane-spanning regions connected by a pore-forming domain, and cytoplasmic N- and C-terminal domains.[8] Northern blot analysis reveals that *KCNJ2* transcripts are present in the human heart, brain, skeletal muscle, placenta, lung, and kidney.[9] In the heart, Kir2.1 greatly contributes to the cardiac inward rectifier K$^+$ current (I_{K1}),[9,10] which determines resting membrane potential and the late phase of action potential repolarization.[11]

Clinical Perspective on p 260

To date, >40 *KCNJ2* mutations have been reported to be responsible for ATS.[5–7,12–15] The use of heterologous expression systems has revealed that most of the mutant *KCNJ2* channels[5,6,12–18] show no whole-cell currents and show dominant-negative effects[5,6,12–14,16,18] or haploinsufficiency.[15,17] Some *KCNJ2* mutations result in intracellular transport failure or a reduced affinity for phosphatidylinositol-4, 5-bisphosphate,

Circ Cardiovasc Genet is available at http://circgenetics.ahajournals.org   DOI: 10.1161/CIRCGENETICS.110.958157
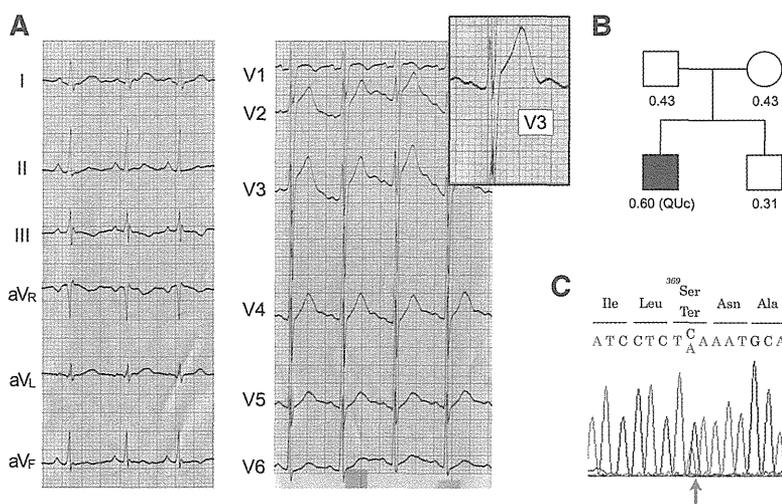
253

Figure 1. A, Twelve-lead ECGs of the proband (the magnified V_3 image is shown as an inset). **B,** Family pedigree. Squares depict male subjects; circle, female subject; open symbols, unaffected members; and solid symbol, affected member. QT intervals are indicated beneath each. **C,** Electropherogram of the sequence surrounding the heterozygous mutation in *KCNJ2* from the patient's genomic DNA.

PIP2.[7,19] The penetrance and severity of the ATS phenotype are extremely variable, which may be partially due to differences in the extent of the functional outcome induced by the mutations.[14] Recently, *KCNJ2* mutations were reported not only in patients with ATS, but also in patients with catecholaminergic polymorphic ventricular tachycardia.[20]

In the present study, we identified a novel nonsense *KCNJ2* mutation, S369X, in a 13-year-old boy who had a prominent QU prolongation and mild muscle weakness but lacked dysmorphic features and examined its functional characterization by using electrophysiological and subcellular distribution analyses.

Methods

Clinical Case

The index patient who reported of muscle weakness and a sense of exhaustion after exercise was referred to our hospital. At the age of 12, he started presenting muscle weakness mainly in his upper limbs and body during hard exercise, which disappeared quickly when he ceased exercise. His ECG showed QU-interval prolongation (QU=0.50 seconds, QUc=0.60) (Figure 1A), whereas the QT interval was not prolonged clearly (QT=0.36 seconds, QTc=0.48).[21] It was sometimes difficult to discriminate the end of the T wave on ECG, but in other recordings of V_3, as shown in the inset of Figure 1A, prominent U waves with increased amplitude (0.15 mV) were observed in V_1 to V_3. The patient has no family history of cardiac sudden death or fatal arrhythmic events (Figure 1B). Resting 12-lead ECGs obtained from all family members presented no abnormalities in QTc and QU interval.

There were no typical periodic paralysis or apparent dysmorphic features in the index patient, and with a suspicion of long QT syndrome (LQTS) or ATS, we conducted the genetic test for *KCNQ1*, *KCNH2*, *SCN5A*, *KCNE1*, *KCNE2*, and *KCNJ2* in 4 family members, including the index patient (Figure 1B). All gave written informed consent for genomic testing. The Ethics Reviewing Committee of Kyoto University approved the protocol in the present study. The investigation conforms with the principles outlined in the Declaration of Helsinki.[22]

Genetic Analysis

Genomic DNA was extracted from peripheral blood lymphocytes using QIAamp DNA midi kits (QIAGEN GmbH; Hilden, Germany). DNA from 302 chromosomes from ethnically matched healthy individuals was used as the control. The entire coding region for each LQTS-related gene was amplified by polymerase chain reaction using primer pairs as previously described,[12] and sequenced using an ABI-Prism 3100 Genetic Analyzer (Applied Biosystems; Foster City, CA).

Mutagenesis and Construction of Plasmids

The wild type (WT) *KCNJ2* clone in the pCMS-enhanced green fluorescent protein (EGFP) expression vector (BD Biosciences Clontech; Franklin Lakes, NJ) was provided by Dr Y. Aizawa (Department of Medicine, Niigata University; Niigata, Japan).[13] For confocal image experiments, WT-*KCNJ2* was subcloned into pIRES1-CD8[10] to coexpress human CD8 as a cell surface marker (WT/CD8). The S369X mutation was generated by site-directed mutagenesis using a QuickChange II XL mutagenesis kit (Stratagene; La Jolla, CA). The primers were 5′-GCAGAAAAGAA-ATATATCCTCTAAAATGCAAATTCATTTTGC-3′ (sense) and 5′-GCAAAATGAATTTGCATTTTAGAGGATATATTTCTTTTC-TGC-3′ (antisense). The sequences of these constructs were confirmed by direct sequencing.

To investigate the subcellular distribution of KCNJ2 channels with laser-scanning confocal microscopy, EGFP was fused to the N-terminus of WT or the mutant *KCNJ2*. The resultant constructs were designated as EGFP-WT and EGFP-S369X, respectively. Lastly, the constructs were subcloned into pcDNA3.1/Zeo(−) (Invitrogen; Carlsbad, CA).

Transient Transfection in Mammalian Cell Lines

For electrophysiological experiments, Chinese hamster ovary (CHO) cells were grown in Dulbecco modified eagle medium supplemented with 20% fetal bovine serum (Nacalai Tesque; Kyoto, Japan), 100 IU/mL penicillin, and 100 μg/mL streptomycin in a 5% CO_2 incubator for 24 hours at 37°C. The cells were plated at 3.0×10^4 cells/35-mm dish for 24 hours before transfection. They were transfected with WT-*KCNJ2* plasmid, S369X-*KCNJ2* plasmid, or both using FuGENE6 (Roche Diagnostics; Indianapolis, IN) as directed by the manufacturer. In confocal microscopy experiments, COS7 cells were seeded at 6.0×10^4 cells/35-mm glass-bottomed microwell dish, grown in Opti-MEM (Invitrogen) for 24 hours at 37°C, and transfected with EGFP-fused *KCNJ2* using LipofectAMINE 2000 (Invitrogen). The medium was removed 24 hours after transfection, and the cells were then incubated in Dulbecco modified eagle medium supplemented with 20% fetal bovine serum for 24 hours at 37°C. Both functional assays were performed 48 hours after transfection.

Electrophysiological Experiments

At 48 hours after transfection, CHO cells expressing WT and mutant KCNJ2 channels were identified by GFP fluorescence using an

A   Kir2.1 WT   Kir2.1 S369X

B

```
              370       380       390       400       410       420
               |         |         |         |         |         |
Human   DLAEKKYILSNANSFCYENEVALTSKEE-DDSENGVPESTSTDTPPDIDLHNQASVPLEPRPLRRESEI
S369X   ·········X
Rat     ····································E·············S··G····················
Mouse   ···································EE·············S··G····················
Guinea Pig ············································-·······························
Chicken ·······························-·EIDT··········H··M·H····G···············
```
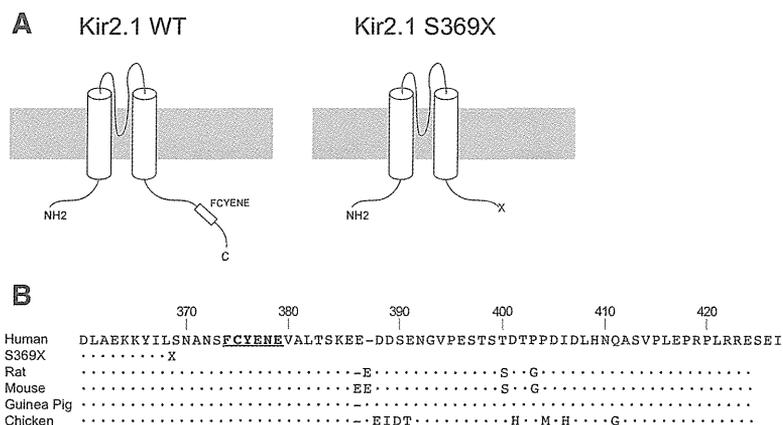
Figure 2. Topology of the Kir2.1 channel. **A**, Kir2.1 subunits are made of 2 transmembrane segments adjacent to a pore-forming loop and cytoplasmic N- and C-termini. On the left, the cytoplasmic C-terminal domain contains a trafficking signal, FCYENE, for efficient export from the endoplasmic reticulum to Golgi (underscored in 2B). On the right, S369X results in a truncation of the C-terminus before the signal. **B**, Alignment of the amino acid sequence of *KCNJ2* around the mutation (S369X) in human, rat, mouse, guinea pig, and chicken. WT indicates wild type.

inverted microscope (Diaphot 300; Nikon; Tokyo, Japan). Whole-cell voltage clamp recordings were performed with patch-clamp techniques using an Axopatch 200A amplifier (Axon Instruments; Foster City, CA) at room temperature. Cells were superfused with a bath solution that contained 150 mmol/L NaCl, 5 mmol/L KCl, 2 mmol/L $CaCl_2$, 1 mmol/L $MgCl_2$, and 10 mmol/L HEPES (pH 7.3, adjusted with NaOH). Pipettes of 2.0 to 5.0 $M\Omega$ were prepared and heat polished before use and were filled with a solution containing 150 mmol/L KCl, 0.5 mmol/L NaCl, 0.5 mmol/L $MgCl_2$, 5 mmol/L EGTA, and 10 mmol/L HEPES (pH 7.3, adjusted with KOH). Data were acquired through a Digidata 1332A digitizer (Axon Instruments) and analyzed with pClamp 9.0 software (Axon Instruments). Currents were elicited by 150-ms pulses applied in 10-mV increments at potentials ranging from −140 to +30 mV from a holding potential of −80 mV.

Laser Scanning Confocal Microscopy

Imaging was performed with an LSM 510-META laser scanning microscope (Carl Zeiss; Thornwood, NY). Confocal images of the fluorescence emitted by GFP were obtained using an argon laser (488 nm) and band pass filter (500 to 550 nm), captured, and manipulated with Zeiss LSM Image Examiner software (Carl Zeiss). GFP fluorescence and CD8 beads-coated with antihuman CD8 antibodies (Dynabeads M-450; Dynal ASA; Oslo, Norway) were used to identify cells expressing both EGFP-WT and EGFP-S369X. To quantify fluorescence distribution changes in cells expressing GFP-fused channel proteins, line-intensity histograms of each image were evaluated.

For analysis of endoplasmic reticulum (ER) colocalization, pDsRed2-ER (BD Biosciences Clontech), which is designed for fluorescent labeling of the ER in living cells, was transfected along with EGFP-WT, EGFP-S369X, or WT-*KCNJ2* pIRES/CD8. DsRed2-ER was excited using the 543-nm line of a helium/neon laser, and the images were collected with a band pass filter (565 to 615 nm).

Fluorescence resonance energy transfer (FRET) has been used as a biological tool to prove the physical interaction of proteins in living cells.[23–26] We used FRET imaging to detect protein-protein interactions between WT and S369X in COS7 with acceptor bleaching,[27] as previously reported.[26] We constructed cyan fluorescent protein (CFP)- or yellow fluorescent protein (YFP)-tagged KCNJ2 using ECFP-N1 or EYFP-N1 vectors (BD Biosciences Clontech), respectively, and cotransfected them to COS7 cells as described previously. FRET efficiency (*E*) was calculated by using the CFP-normalized fluorescence intensity before (I_{DA}) and after (I_D) photobleaching of the acceptor (YFP) as follows:

$$E = [(I_D - I_{DA})/I_{DA}](\times 100)^{26}$$

Statistical Analysis

Data were presented as the mean±SEM. For nonparametric variables, correlation was tested by the Wilcoxon, Kruskal-Wallis, or Spearman rank test. $P < 0.01$ was considered significant in all analyses.

Results

De Novo *KCNJ2* Mutation in ATS

Genetic analyses for the aforementioned LQTS-related genes in the proband were all negative except *KCNJ2*. An analysis for *KCNJ2* revealed the presence of a heterozygous C>A substitution at nucleotide 1106 (Figure 1C, arrow). The change was not identified in his family members (Figure 1B) or in 302 unaffected healthy individuals, indicating that it is a novel and de novo mutation. The mutation resulted in the introduction of a premature stop codon at S369 (S369X), which leads to the loss of 59 amino acids at the C-terminus and a truncation of the KCNJ2 channel protein (Figure 2A). The 59 amino acids that follow serine 369 are highly conserved among various species (Figure 2B). This C-terminal segment contains a distinct ER-to-Golgi forward-trafficking signal (FCYENE indicated by boldface letters in Figure 2B), which is essential for export of the channel protein from the ER to the Golgi.[28] Therefore, the lack of this motif may cause the sequestration of KCNJ2 within the ER.

Electrophysiological Properties of KCNJ2-WT and KCNJ2-S369X

To assess functional outcome of the truncated KCNJ2 subunits, we conducted whole-cell voltage-clamp recordings as described in the Methods section. CHO cells transfected with 1 μg of WT exhibited robust inward currents at test potentials below −80 mV and outward currents rectified between −80 and −10 mV (Figure 3A and 3D), which were similar to typical I_{K1} as previously reported.[9,10] S369X subunits when expressed alone (1 μg), however, showed significantly smaller currents (WT versus S369X, −542±46 versus −83.5±13.5 picoamperes per picofarad [pA/pF] at −140 mV, $P < 0.0001$, n=19 and n=15, respectively) (Figure 3B, 3D, and 3E). $BaCl_2$ (0.5 mmol/L) reversibly blocked both WT and S369X channel currents (Figure 3A and 3B, bottom). To mimic the genetic condition in the proband, cells were cotransfected with both WT and S369X at an equimolar ratio (0.5 μg each) (Figure 3C through 3E), which displayed ≈61% of the current densities of those expressing WT alone
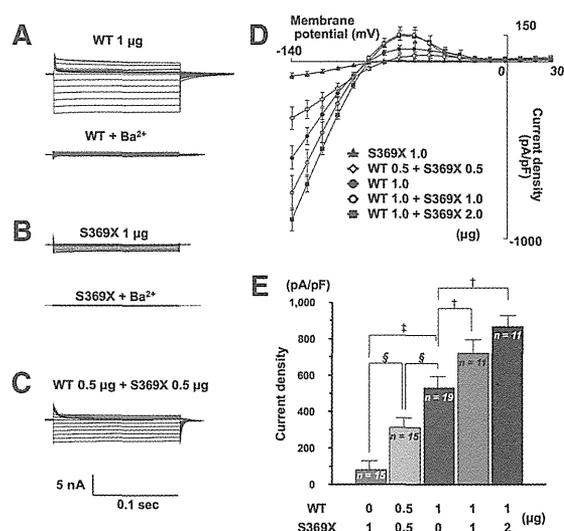
Figure 3. Functional assay of KCNJ2–S369X in Chinese hamster ovary (CHO) cells. Representative whole-cell currents elicited by 10-mV test pulses ranging from −140 to +30 mV from a holding potential of −80 mV was recorded in cells transfected with WT (1 μg) (**A**), S369X (1 μg) and blocked with Ba^{2+} (0.5 mmol/L) (**B**), and WT (0.5 μg) and S369X (0.5 μg) (**C**). Extracellular application of 0.5 μg Ba^{2+} completely blocked the reconstituted I_{K1}-like currents to the right of **A** and **B**. **D**, Current-voltage relationships of whole-cell currents in CHO cells expressing the S369X mutant (1 μg), WT (0.5 μg)+S369X (0.5 μg), WT alone (1 μg), WT (1 μg)+S369X (1 μg), and WT (1 μg)+S369X (2 μg). Currents were recorded at test potentials ranging from −140 to 30 mV for 150 ms in 10-mV steps from a holding potential of −80 mV. **E**, Averages of peak current densities were measured at −140 mV in CHO cells transfected with WT and S369X at various ratios. Numbers within the bars indicate the number of observations. The values of the 5 groups were significantly different ($P<0.001$) by Kruskal-Wallis test. †$P<0.001$ by Spearman rank correction coefficient. ‡$P<0.0001$ by Wilcoxon test. §$P<0.001$ by Wilcoxon test. pA/pF indicates picoamperes per picofarad; WT, wild type.

(1 μg) (−330±40 pA/pF at −140 mV, $P<0.001$ versus WT and $P<0.001$ versus S369X, n=15) (Figure 3E). These WT/S369X currents also were inhibited by $BaCl_2$ (0.5 mmol/L) (data not shown). These results suggest that there is no dominant-negative suppression by S369X subunits, which sharply contrasts the results from many other mutants.[5–7,12–14,17,18,29]

Supposing no functional interaction between WT and S369X, the current density of WT/S369X (1 μg each) should increase by ≈16% compared to that of WT (1 μg) alone because cells expressing S369X (1 μg) alone showed ≈16% of the current density produced by WT 0.5 μg (Figure 3E). However, the cells transfected with WT/S369X (1 μg each) (Figure 3E) showed a significantly larger current density, increased by ≈33% to that of WT (1 μg) alone (WT 1 μg+S369X 1 μg, −724±98 pA/pF, n=11; WT 1 μg alone, −542±46 pA/pF, n=19; at −140 mV; $P<0.001$). Moreover, increasing S369X mutant to 2 μg (Figure 3E) promoted but did not reduce resultant currents (−869±63 pA/pF, n=11, $P<0.001$ versus WT 1 μg alone). Thus, electrophysiological analyses suggest that WT channel subunits are capable of

rescuing KCNJ2-S369X subunit function, presumably through direct association.

Subcellular Distribution of KCNJ2-WT and KCNJ2-S369X

To test whether mutant Kir2.1 subunits are trafficking refractory, confocal microscopic analyses were conducted using EGFP-fused Kir2.1 channels. Fusion of EGFP to the N-terminus of Kir2.1 (EGFP-WT) does not affect the electrophysiological properties of Kir2.1 because EGFP-WT fusions are functional and show an I-V relationship similar to that of WT (data not shown). Current densities of EGFP-WT at −140 mV (−584.9±45 pA/pF, n=12) were not significantly different from those of WT ($P=0.50$).

Figure 4 shows representative confocal microscopic images obtained from COS7 cells expressing EGFP-WT, EGFP-S369X, and EGFP-S369X+WT. The top 2 rows show phase-contrast microscopic and confocal images from successfully transfected cells. The distribution of GFP signal from WT was consistent with the localization of the channel in the plasma membrane. In contrast, cells expressing EGFP-S369X did not clearly exhibit fluorescence in the membrane, and the signal was mainly localized to the cytoplasm. Because S369X had no dominant-negative effect on WT in electrophysiological experiments, we then examined the interaction between WT and S369X (Figure 4). Cotransfection with non-GFP-tagged WT exhibited a mixed distribution pattern in both the plasma membrane and the cytoplasm.

Line intensity histograms are shown in the bottom row of Figure 4. Line intensity (indicated as black [intermitted light] and green [fluorescence]) was detected along the lines illustrated in the third row of magnified images. This analysis confirmed that GFP signals from WT were strongest in the membrane (arrow), and those from EGFP-S369X were retained mainly in the cytoplasm, but cotransfection of non-GFP-tagged WT altered its distribution to the plasma membrane (arrow indicates the GFP signal from the membrane). Thus, WT-KCNJ2 subunits rescued mutant channel proteins and assisted their transport to the cell membrane.

It is most plausible that the mutant S369X remained in the ER because it lacked the ER export motif. We then examined the location of EGFP-S369X proteins by using an ER-specific marker, DsRed2-ER (Figure 5). EGFP-WT appeared to express on the plasma membrane (Figure 5A-1). It is more evident when this image is merged with that detecting ER localization (Figure 5A-2 and 5A-3). In contrast, EGFP-S369X (Figure 5B-1) mostly colocalized with DsRed2-ER (Figure 5B-2). There was scarce expression of the S369X mutant in the plasma membrane (Figure 5B-3). Finally, cotransfection with nontagged WT resulted in a modest, but evident expression of S369X mutant in the cell membrane (reappearance of GFP signal), strongly suggesting that WT rescued the trafficking of S369X proteins to the membrane (Figure 5C-1 through 5C-3).

To prove a direct interaction between WT and S369X subunits, the FRET imaging technique was used along with the acceptor bleaching method (Figure 6). When CFP-S369X was coexpressed with YFP-WT, both were colocalized as shown in the merged images (Figure 6A). After YFP bleach-
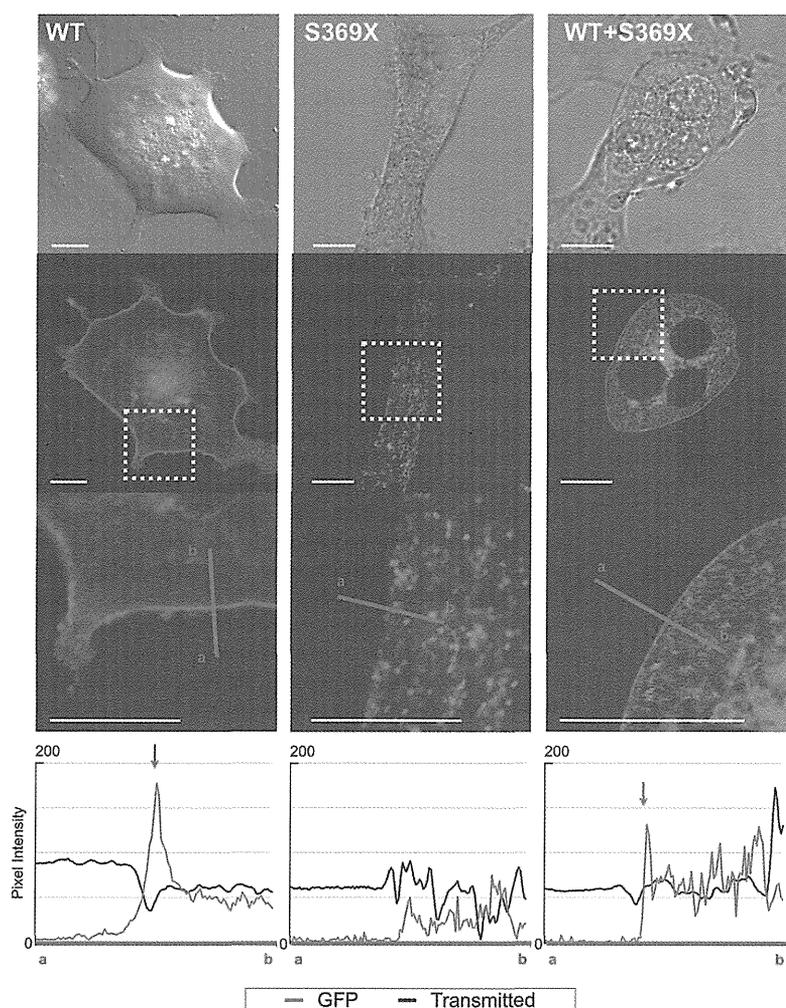
Figure 4. Subcellular distribution of WT and S369X in COS7 cells. Representative microscopic images of COS7 cells expressing EGFP-WT (1 μg/dish), EGFP-S369X (1 μg/dish), and EGFP-S369X cotransfected with WT-*KCNJ2* pIRES/CD8 (0.5 μg each/dish) (bars, 20 μm). The first row shows contrast microscopic images and the second, the corresponding confocal microscopic images. The third row shows magnified images of the boxed areas in the second row. The fourth row shows quantification of pixel intensity along the lines shown in the third row for GFP (green) and transmitted light (black). EGFP indicates enhanced green fluorescent protein WT, wild type.

ing, there was a significant and consistent increase in CFP fluorescence intensity in the cytoplasm as shown in Figure 6B. These findings indicate that CFP-S369X physically interacts with the WT subunits in an intracellular compartment. Figure 6C shows the FRET efficiency obtained from 10 independent experiments for a given experimental condition. As shown in Figure 6C, for negative controls, CFP-WT alone and CFP-N1+YFP-N1 were used. The FRET efficiency between WT and mutant was significantly larger than that of the negative controls ($P<0.01$ versus WT-CFP, $P<0.01$ versus CFP-N1+YFP-N1). The FRET efficiency between CFP-WT and YFP-WT were examined as a positive control and showed a similar FRET efficiency to CFP-S369X/YFP-WT. Exchange of labeled fluorescence for each other (ie, CFP-WT and YFP-S369X) also yielded a large and similar value, indicating the direct interaction between WT and the mutant subunits.

Discussion

In the present study, we report a novel nonsense *KCNJ2* mutation, S369X, in a patient with a prominent QU prolon-

gation and mild ATS phenotype. To our knowledge, this report is the first of a nonsense mutation resulting in truncated KCNJ2 channel subunits. Electrophysiological experiments revealed that mutant channels showed significantly smaller currents and did not exhibit dominant-negative effects on WT. Confocal microscopic imaging showed that the EGFP-fused S369X channel is mainly retained inside the cell and that coexpression with KCNJ2-WT partially restored the cell surface expression of the mutant proteins.

Loss-of-function type *KCNJ2* mutations are known to be responsible for ATS.[5,6,12–14,16–18] The *KCNJ2* mutations reported previously in ATS are nonfunctional and have dominant-negative effects (ie, the mutant subunits suppressed the WT subunits' function[5,6,12–14]). S369X showed no dominant-negative effects, which may explain why the index patient exhibited a relatively mild form of ATS without ventricular tachyarrhythmia or dysmorphic features. Because the truncation occurs at the very end of the C-terminus, it is suggested that the structure of the pore region would be preserved, and therefore, proteins containing the truncated subunit could partially function as WT (Figure 3B).